

A modal-based Partition of Unity Finite Element Method for layered wave propagation problems

P. Destuynder^a, L. Hervella-Nieto^b, P. M. López-Pérez^c, J. Orellana^d, A. Prieto^{b,*}

^a *Laboratoire des Sciences de l'Ingénieur pour l'Environnement - LaSIE. France*

^b *CITIC. Department of Mathematics. Universidade da Coruña. Spain*

^c *Department of Applied Mathematics. IMUVA and Faculty of Science. Universidad de Valladolid. Spain*

^d *Conservatoire National des Arts et Metiers. Paris, France*

Abstract

The time-harmonic propagation of waves in layered media is simulated numerically by means of a modal-based Partition of Unity Finite Element Method (PUFEM). Instead of using typical plane wave or Bessel solutions of the Helmholtz equation to design the discretization basis, the proposed modal-based PUFEM uses explicitly the tensor-product expressions of the eigenmodes (the so-called Love and interior modes) of a spectral transverse problem, which fulfil the coupling conditions among layers. This modal-based PUFEM approach does not introduce quadrature errors since the coefficients of the discrete matrices are computed in closed-form. An preliminary analysis of the high condition number suffered by the proposed method is also analysed in terms of the mesh size and the number of eigenmodes involved in the discretization. The numerical methodology is validated through a number of test scenarios, where the reliability of the proposed PUFEM method is discussed by considering different modal basis and source terms. Finally, some indicators are introduced to select a convenient discrete PUFEM basis taking into account the observability of cracks placed on a coupling boundary between two adjacent layers.

Keywords: Partition of Unity Finite Element Method, layered material, modal decomposition

1. Introduction

The development of engineering tools to find cracks on the interfaces between different layers materials is fundamental to the early detection of defects in some widely used mechanical structures in industry (for example, pipes with a coating [29], multilayer panels in aeronautic shields [8]). Currently, ultrasonic testing [4] and Foucault currents [1] propagating transversally through the coupling interfaces are common inspection techniques. In both cases, their effectiveness and practical application is limited by the fact that the excitation source must be placed close to the crack location for its correct detection. In order to overcome that limitation, the use of Love waves to find a defect far from the source has been recently analysed (see, for instance, [12, 16, 28],

*Corresponding author. Phone: +34 881016004

Email addresses: philippe.destuynder@univ-lr.fr (P. Destuynder), luis.hervella@udc.es (L. Hervella-Nieto), paulamaria.lopez@uva.es (P. M. López-Pérez), jose.orellana@lecnam.net (J. Orellana), andres.prieto@udc.es (A. Prieto)

and references therein). In this framework, Love modes are surface waves associated with the coupling interface, whose motion is transverse to the direction of wave propagation (see [25] for a detailed description).

To achieve high crack detection rates by using Love waves (see [9]), it is crucial the *a priori* knowledge of a high accurate prediction of the mechanical behaviour of the problem without a crack. However, typical numerical approximations based on finite differences or finite element methods suffer from the numerical pollution effects at high frequency regime [15], where despite the grid or the mesh could be refined enough to capture the wave-like oscillations of the model solution, the accumulation of phase-lag errors introduce spurious deviations on the approximated numerical results [14]. Other high-order techniques such as high-order or spectral finite element methods [3, 11] could mitigate these numerical pollution phenomena but they still involve a high computational cost since the mesh used in the discretization problem should be conformal with respect to the internal coupling interfaces of the multilayered media [26].

The present work is focused on the numerical approximation of the solution of a non-destructive testing problem involving a bilayered medium without the presence of a crack. The proposed numerical method deals with both challenging drawbacks described above. For this purpose, Love and interior modes (computed in closed-form from a simplified auxiliary transverse problem) are used in combination with a partition of unity finite element method (PUFEM) discretization. This approach avoids any undesirable numerical pollution effects [13] and simultaneously does not require the use of refined meshes to obtain accurate numerical results even in the case of considering thin layers.

The family of PUFEM methods was introduced in [21], where the standard polynomial-based discretization of a classical finite element method (FEM), is used as a partition of unity. In that manner, instead of computing a polynomial approximation of the exact solution, every local polynomial basis is multiplied by an exact solution of a target model leading to an *enriched* discrete space where some exact local solutions of the model are naturally included. Typically, in the case of the two-dimensional Helmholtz model stated in a homogeneous medium (with a constant wavenumber), this enrichment procedure involves the multiplication of piecewise polynomial functions (defined on a triangular mesh) by plane waves [17, 22, 24], radial solutions (written in terms of Bessel functions) [22], or two-dimensional eigenfunctions [2]. Further developments on the use of the PUFEM technique applied to heterogeneous media have been analysed recently (see [7] and [20]). However, those approaches use conformal meshes with respect to the position of the coupling interfaces, and since the enriched functions used in the discretization are only local solutions within a particular layer of the model, special treatments are required to impose the coupling conditions among layers.

For the application of the proposed approach, the compatibility between the system of spatial coordinates used to write the mechanical model (in this case, the Helmholtz equation) and the mathematical description of the coupling boundaries of the layered material plays a key role. More precisely, it is assumed that: (H1) the global governing partial differential equation (holding in the entire computational domain) involves some piecewise (constant per layer) coefficients and (H2) this equation admits a tensorial representation such that the normal and tangential spatial coordinates with respect to the coupling boundaries can be identified. For instance, such assumptions are usually fulfilled in isolation sandwich panels utilized in building acoustics (where a Cartesian system of coordinates is used and the coupling boundaries are planar) or in pipelines with coatings (where cylindrical coordinates are applied to be compatible with the curved coating shape).

Thanks to both assumptions (H1)-(H2) written above, the enriched modal-based PUFEM discretization can be designed as tensor products by using a splitting of eigenmodes derived from an auxiliary spectral problem in the normal direction and a standard piecewise polynomial basis acting on the tangential coordinates. For the sake of simplicity in the exposition, this work is focused on a Cartesian system of spatial coordinates in a two-dimensional setting, where a bilayered material with planar coupling boundaries is studied.

The outline of this manuscript is as follows: the model problem and its variational formulation is presented in Section 2. In Section 3, the computation of Love and interior modes is described in a detailed and pedagogical manner from an auxiliary spectral problem. The description of the modal-based PUFEM approach, its associated discrete problem, and its matrix description is included Section 4. Additionally, an analysis of the condition number of the PUFEM stiffness matrix is included. Section 5 includes a wide variety of numerical tests in order to illustrate the numerical behaviour of the proposed modal-based PUFEM method. Finally, a criterion to identify a convenient combination of Love and interior modes in the PUFEM basis is described in Section 6 and some conclusions are discussed in Section 7.

2. Model problem

Throughout this work, a bilayered elastic material domain will be considered, where an excitation will be imposed to polarize both layers transversally. So, the computational domain $\Omega \subset \mathbb{R}^2$ is split in two layers, denoted respectively by Ω_+ and Ω_- , where different physical properties are settled. More precisely, the transverse propagation speed c is defined as a piecewise-constant function given by

$$c(\mathbf{x}) = \begin{cases} c_+ & \text{if } \mathbf{x} \in \Omega_+, \\ c_- & \text{if } \mathbf{x} \in \Omega_-, \end{cases}$$

where it is assumed $0 < c_- < c_+$. In addition, the exterior boundary of the computational domain Ω is split in four disjoint parts, $\partial\Omega = \Gamma_e \cup \Gamma_s \cup \Gamma_+ \cup \Gamma_-$.

Under the assumptions of small perturbations of the displacement field and the stress tensor, the mechanical vibrations of bilayered structures can be modelled by a linear elastic mode, where only the transverse component of the displacement field is involved. Taking into account a frequency domain model, i.e., if the external forces are harmonic in time with frequency $\omega > 0$, the time-harmonic problem is stated as follows: *Find the displacement field $u : \Omega \rightarrow \mathbb{C}$ such that it holds*

$$-\omega^2 u - \operatorname{div}(c^2 \nabla u) = f \quad \text{in } \Omega_+ \cup \Omega_-, \quad (1)$$

$$c^2 \frac{\partial u}{\partial \boldsymbol{\nu}} = g \quad \text{on } \Gamma_+ \cup \Gamma_-, \quad (2)$$

$$-i\omega\beta u + c \frac{\partial u}{\partial \boldsymbol{\nu}} = r \quad \text{on } \Gamma_e \cup \Gamma_s, \quad (3)$$

$$u|_{\Omega_-} = u|_{\Omega_+} \quad \text{on } \Gamma_I, \quad (4)$$

$$c_-^2 \frac{\partial u}{\partial \boldsymbol{\nu}} \Big|_{\Omega_-} = c_+^2 \frac{\partial u}{\partial \boldsymbol{\nu}} \Big|_{\Omega_+} \quad \text{on } \Gamma_I, \quad (5)$$

where f, g , and r are respectively volumetric and surface external loads. Here $\boldsymbol{\nu}$ denotes the unit normal vector outwards to Ω_- and $\Gamma_I = \overline{\Omega_+} \cap \overline{\Omega_-}$ is the coupling boundary. It is straightforward

to derive the variational formulation of this frequency-domain problem: For given $\omega > 0$, find $u \in H^1(\Omega)$ such that

$$A_\beta(u, \phi) - \omega^2 \int_\Omega u \bar{\phi} \, d\mathbf{x} = L(\phi) \quad (6)$$

for all $\phi \in H^1(\Omega)$, with

$$\begin{aligned} A_\beta(u, \phi) &= \int_\Omega c^2 \nabla u \cdot \nabla \bar{\phi} \, d\mathbf{x} - i\omega\beta \int_{\Gamma_e \cup \Gamma_s} c u \bar{\phi} \, d\sigma, \\ L(\phi) &= \int_\Omega f \bar{\phi} \, d\mathbf{x} + \int_{\Gamma_+ \cup \Gamma_-} g \bar{\phi} \, d\sigma + \int_{\Gamma_e \cup \Gamma_s} c r \bar{\phi} \, d\sigma. \end{aligned}$$

All variational terms in this weak problem are well-posed assuming that $f \in L^2(\Omega)$, and the boundary loads $r \in H^{-\frac{1}{2}}(\Gamma_e \cup \Gamma_s)$ and $g \in H^{-\frac{1}{2}}(\Gamma_+ \cup \Gamma_-)$. The main goal of the present work is the description of a modal-based PUFEM method to solve the variational problem (6) in a bilayered setting. With this purpose, a basis consisting in eigenmodes of an auxiliary spectral problem will be computed in the sections below.

3. Spectral characterization of the auxiliary problem

The key ingredient on the modal-based PUFEM discretization consists in the computation of closed-form expressions for the eigenvalues and eigenfunctions of an auxiliary problem involving the same partial differential equations and coupling conditions introduced in the target problem (1)-(5), but possibly with different boundary conditions on the outer boundaries. In that manner, the use of an eigenmode expansion for the solution of target problem (1)-(5) could be challenging an potentially it would exhibit a poor asymptotic convergence with respect to the number of modes used (since the target problem (1)-(5) could not be associated with a self-adjoint compact resolvent operator). However, since the auxiliary problem will be stated in such a way that its eigenmodes form a complete functional L^2 -basis, they will provide a suitable functional setting to be combined locally with a partition of unity method.

In what follows, the spectral characterization of this new global problem is analysed, where the Robin boundary conditions with $\beta \neq 0$ in problem (1)-(5) are replaced for simpler Neumann boundary conditions (with $\beta = 0$), this is: Finding the eigenpairs (w, λ) , $w \neq 0$, such that

$$\lambda w - \operatorname{div}(c^2 \nabla w) = 0 \quad \text{in } \Omega, \quad (7)$$

$$\frac{\partial w}{\partial \nu} = 0 \quad \text{on } \partial\Omega, \quad (8)$$

$$w|_{\Omega_-} = w|_{\Omega_+} \quad \text{on } \Gamma_I, \quad (9)$$

$$c_-^2 \frac{\partial w}{\partial \nu} \Big|_{\Omega_-} = c_+^2 \frac{\partial w}{\partial \nu} \Big|_{\Omega_+} \quad \text{on } \Gamma_I. \quad (10)$$

In comparison with the original model problem (1)-(5), this auxiliary problem (7)-(10) have Neumann boundary conditions on $\partial\Omega$ and hence, the linear resolvent operator associated to this spectral problem is self-adjoint and compact. Hence, a standard spectral analysis shows there is an infinity numerable set of positive eigenvalues $\{\lambda_{n,j}\}_{n,j \in \mathbb{N}}$ (without any accumulation point), which are as-

sociated with the angular resonance frequencies $\omega_{n,j} = i\sqrt{\lambda_{n,j}}$ (see a detailed analysis in [19] for further details).

3.1. Spectral analysis in the Cartesian system of coordinates

Despite the present modal-based PUFEM discretization is applicable to a wide variety of computational domains and different governing partial differential equations, both the geometry and the equations must be suitable for a description in a general local orthogonal system of coordinates (such as polar or more general convex coordinates) fulfilling hypothesis (H1)-(H2). For simplicity on the method description in this manuscript, a standard Cartesian system of coordinates is used to introduce the computational domain. More precisely, throughout this work, a bilayered computational domain is considered. More precisely, the layered media is given by $\Omega = (-a, H) \times (0, L)$ with $a, L, H > 0$, and the upper and lower layers are $\Omega_+ = (0, H) \times (0, L)$ and $\Omega_- = (-a, 0) \times (0, L)$, respectively (see Figure 1).

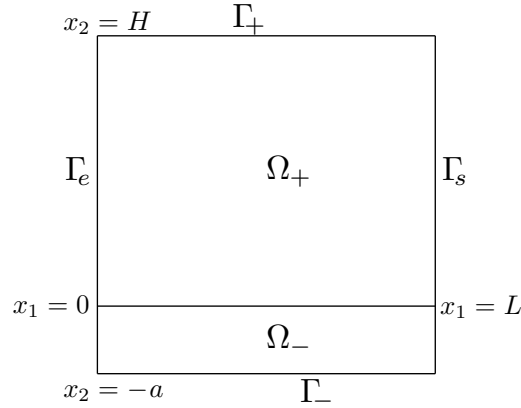


Figure 1: Computational domain of the bilayered elastic material described in terms of the Cartesian coordinates (x_1, x_2) .

Under assumptions (H1)-(H2), the analytic computation of the eigenpairs can be performed by a classical separation of variables procedure. Then, if the non-null eigenfunctions are given by $w(x_1, x_2) = q(x_1)p(x_2)$, and since the profile of the speed of sound c is piecewise constant, then the Helmholtz equation in Ω_+ leads to $-c_+^2 q'' p - c_+^2 p'' q = \lambda q p$. Since q and p depends on an unique spatial variable, there exists a constant μ such that

$$q'' + \mu q = 0 \quad \text{in } (0, L) \quad \text{and} \quad -c_+^2 p'' - (\lambda - c_+^2 \mu) p = 0 \quad \text{in } (0, H).$$

Similar arguments can be performed for $\Omega_- = (0, L) \times (-a, 0)$. In both cases, the differential equation satisfied by q is given by $q'' = \mu q$, which is completed with the homogeneous Neumann boundary conditions at $x_1 = 0$ and $x_1 = L$. Straightforward computations show that there exists a sequence of eigenpairs $\{(\mu_n, q_n)\}_{n \in \mathbb{N}}$ (normalized with respect the $L^2(0, L)$ norm) defined by

$$q_0(x_1) = \sqrt{\frac{1}{L}}, \quad \mu_0 = 0, \tag{11}$$

$$q_n(x_1) = \sqrt{\frac{2}{L}} \cos(\sqrt{\mu_n} x_1), \quad \mu_n = \left(\frac{n\pi}{L}\right)^2, \quad n \in \mathbb{N}, n \neq 0. \tag{12}$$

For each eigenpair (μ_n, q_n) , the x_2 -dependent factor $p = p_n$ must be computed. If the differential equation satisfied by p_n is completed with the homogeneous Neumann boundary conditions at $x_2 = -a$ and $x_2 = H$, each p_n satisfies

$$-(c^2 p_n')' - (\lambda_n - c^2 \mu_n) p_n = 0 \quad \text{in } (-a, 0) \cup (0, H), \quad (13)$$

$$p_n'(-a) = p_n'(H) = 0, \quad (14)$$

$$p_n(0^+) = p_n(0^-), \quad (15)$$

$$c_+^2 p_n'(0^+) = c_-^2 p_n'(0^-). \quad (16)$$

For each fixed value of $n \in \mathbb{N}$, there exist a sequence of eigenpairs $\{(\lambda_{n,j}, p_{n,j})\}_{j \in \mathbb{N}}$ which are solution of the spectral differential problem (13)-(16). To describe them explicitly, two different cases should be considered: Love and interior modes. In what follows, it is shown that the eigenpairs $\{(\lambda_{n,j}, w_{n,j})\}_{n,j \in \mathbb{N}}$ of the auxiliary spectral problem (7)-(8) are given by $w_{n,j}(x_1, x_2) = q_n(x_1) p_{n,j}(x_2)$, where q_n are defined by (11)-(12) and $p_{n,j}$ are computed in closed form.

3.1.1. Love modes

First, those eigenmodes which can be understood as interface modes, also called Love modes. They satisfy $\mu_n c_-^2 < \lambda_{n,j} < \mu_n c_+^2$, and hence they are solutions of Equation (13), which can be written as

$$p_{n,j}(x_2) = \begin{cases} C_1 \cos(K_-^{n,j}(x_2 + a)) + C_2 \sin(K_-^{n,j}(x_2 + a)) & \text{if } x_2 \in (-a, 0), \\ D_1 \cosh(K_+^{n,j}(x_2 - H)) + D_2 \sinh(K_+^{n,j}(x_2 - H)) & \text{if } x_2 \in [0, H), \end{cases}$$

being C_1, C_2, D_1 and D_2 constants to be determined and where the positive wave numbers in each subdomain are given by

$$K_-^{n,j} = \sqrt{\mu_n \left(\left(\frac{\xi_{n,j}}{c_-} \right)^2 - 1 \right)}, \quad K_+^{n,j} = \sqrt{\mu_n \left(1 - \left(\frac{\xi_{n,j}}{c_+} \right)^2 \right)}, \quad (17)$$

with $\xi_{n,j} = \sqrt{\lambda_{n,j} / \mu_n}$ and variables $\xi_{n,j} \in (c_-, c_+)$. The Neumann boundary conditions (14) lead to $C_2 = D_2 = 0$. Applying now the interface conditions (15)-(16) in order to find C_1 and D_1 , the following linear system of equations has to be solved

$$\begin{cases} C_1 \cos(K_-^{n,j} a) = D_1 \cosh(K_+^{n,j} H), \\ C_1 K_-^{n,j} \sin(K_-^{n,j} a) = D_1 K_+^{n,j} \sinh(K_+^{n,j} H). \end{cases} \quad (18)$$

To enforce the determinant of the matrix in system (18) is null, the following dispersion equation must be fulfilled:

$$\frac{c_+}{c_-} \sqrt{\frac{c_+^2 - (\xi_{n,j})^2}{(\xi_{n,j})^2 - c_-^2}} \tanh \left(H \sqrt{\mu_n \left(1 - \left(\frac{\xi_{n,j}}{c_+} \right)^2 \right)} \right) = \tan \left(a \sqrt{\mu_n \left(\left(\frac{\xi_{n,j}}{c_-} \right)^2 - 1 \right)} \right). \quad (19)$$

As the linear system (18) has multiple solutions, it is chosen $C_1 = \cos(K_-^{n,j} a)^{-1}$ and then, from the first equation in (18), it can be deduced that $D_1 = \cosh(K_+^{n,j} H)^{-1}$. Consequently, the eigenfunctions $p_{n,j}$ (normalized to satisfy $p_{n,j}(0) = 1$) are given by

$$p_{n,j}(x_2) = \begin{cases} \frac{\cos(K_-^{n,j}(x_2 + a))}{\cos(K_-^{n,j} a)} & \text{if } x_2 \in (-a, 0), \\ \frac{\cosh(K_+^{n,j}(x_2 - H))}{\cosh(K_+^{n,j} H)} & \text{if } x_2 \in [0, H]. \end{cases} \quad (20)$$

3.1.2. Interior modes

The second type of eigenmodes are the interior modes. They correspond to those eigenmodes whose associated eigenvalue satisfies $\lambda_{n,j} > \mu_n c_+^2$. Having into account this condition, the solutions of equation (13) for this case can be written as follows:

$$p_{n,j}(x_2) = \begin{cases} \tilde{C}_1 \cos(\tilde{K}_-^{n,j}(x_2 + a)) + \tilde{C}_2 \sin(\tilde{K}_-^{n,j}(x_2 + a)) & \text{if } x_2 \in (-a, 0), \\ \tilde{D}_1 \cos(\tilde{K}_+^{n,j}(x_2 - H)) + \tilde{D}_2 \sin(\tilde{K}_+^{n,j}(x_2 - H)) & \text{if } x_2 \in [0, H], \end{cases}$$

being $\tilde{C}_1, \tilde{C}_2, \tilde{D}_1$ and \tilde{D}_2 constants to be determined and where the positive wave numbers in each subdomain are given by

$$\tilde{K}_-^{n,j} = \sqrt{\mu_n \left(\left(\frac{\zeta_{n,j}}{c_-} \right)^2 - 1 \right)}, \quad \tilde{K}_+^{n,j} = \sqrt{\mu_n \left(\left(\frac{\zeta_{n,j}}{c_+} \right)^2 - 1 \right)}. \quad (21)$$

In the expressions written above $\zeta_{n,j} = \sqrt{\lambda_{n,j}/\mu_n}$ and hence $\zeta_{n,j} \in (c_+, +\infty)$. The Neumann boundary conditions (14) lead to $\tilde{C}_2 = \tilde{D}_2 = 0$. Applying now the interface conditions (15)-(16) in order to find \tilde{C}_1 and \tilde{D}_1 , the following system has to be solved:

$$\begin{cases} \tilde{C}_1 \cos(\tilde{K}_-^{n,j} a) = \tilde{D}_1 \cos(\tilde{K}_+^{n,j} H), \\ -\tilde{C}_1 \tilde{K}_-^{n,j} \sin(\tilde{K}_-^{n,j} a) = \tilde{D}_1 \tilde{K}_+^{n,j} \sin(\tilde{K}_+^{n,j} H). \end{cases} \quad (22)$$

Again, to ensure that the determinant of the matrix in system (22) is null, the following dispersion equation must be fulfilled

$$\frac{c_+}{c_-} \sqrt{\frac{(\zeta_{n,j})^2 - c_+^2}{(\zeta_{n,j})^2 - c_-^2}} \tan \left(H \sqrt{\mu_n \left(\left(\frac{\zeta_{n,j}}{c_+} \right)^2 - 1 \right)} \right) + \tan \left(a \sqrt{\mu_n \left(\left(\frac{\zeta_{n,j}}{c_-} \right)^2 - 1 \right)} \right) = 0. \quad (23)$$

As the linear system (22) has multiple solutions, it is chosen that $\tilde{C}_1 = \cos(\tilde{K}_-^{n,j} a)^{-1}$ and then, from the first equation in (22), it can be deduced that $\tilde{D}_1 = \cos(\tilde{K}_+^{n,j} H)^{-1}$. So in this case, the

eigenfunctions $p_{n,j}$ (normalized to satisfy $p_{n,j}(0) = 1$) are given by

$$p_{n,j}(x_2) = \begin{cases} \frac{\cos(\tilde{K}_-^{n,j}(x_2 + a))}{\cos(\tilde{K}_-^{n,j}a)} & \text{if } x_2 \in [-a, 0], \\ \frac{\cos(\tilde{K}_+^{n,j}(x_2 - H))}{\cos(\tilde{K}_+^{n,j}H)} & \text{if } x_2 \in [0, H]. \end{cases} \quad (24)$$

Figure 2 illustrates two different kind of eigenmodes, a Love mode (left plot) and an interior mode (right plot) with respect to the x_2 -axis through the computational domain Ω (see 1). The speed of sound has been settled to $c_- = 1/2$ in Ω_- and $c_+ = 1$ in Ω_+ . In this example, the geometrical dimensions of the computational domain are given by $L = 1$, $a = 0.2$ and $H = 0.8$. The Love eigenmode $w_{n,j}$ (with $n = 15$ and $j = 5$) has an oscillatory behaviour in $(-a, 0)$ and decays exponentially in $(0, H)$, as it can be observed in the left plot. The right plot illustrates the interior eigenmode with $n = 15$ and $j = 5$. It has an oscillatory behaviour in the whole domain, although the oscillation changes when the wave crosses the interface at $x_2 = 0$.

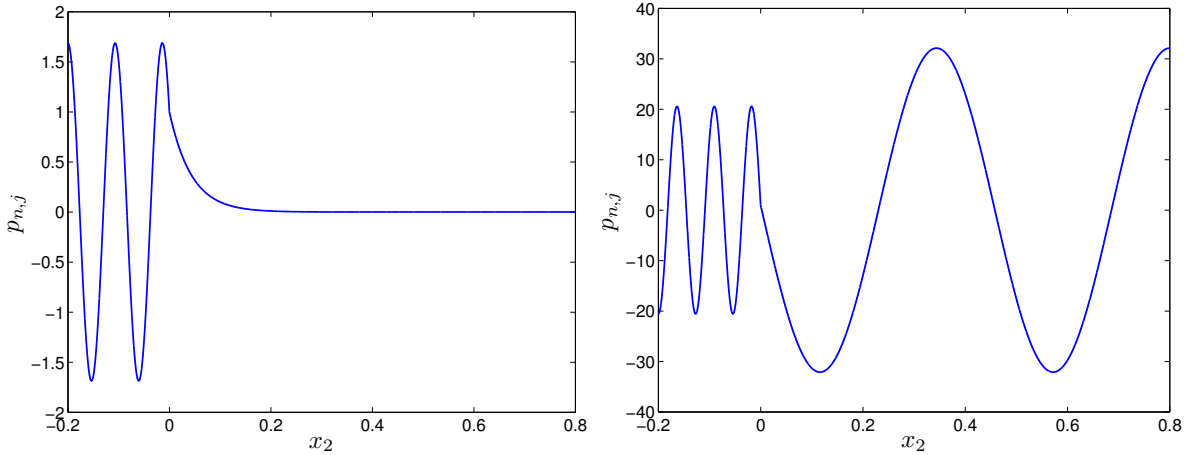


Figure 2: Love mode $p_{n,j}$ from equation (20) (left) and interior mode $p_{n,j}$ from equation (24) (right) plotted with respect to x_2 , for $n = 15$ and $j = 5$. It can be observed the exponential decay of the Love mode and the oscillatory behaviour of the interior mode in $(0, H)$, being $H = 0.8$.

Note that the eigenmodes whose eigenvalue satisfies $\lambda_{n,j} < \mu_n c_-^2$ are not considered, because the dispersion equation that should be fulfilled is

$$\frac{c_+}{c_-} \sqrt{\frac{c_+^2 - (\xi_{n,j})^2}{c_-^2 - (\xi_{n,j})^2}} \tanh \left(H \sqrt{\mu_n \left(1 - \left(\frac{\xi_{n,j}}{c_+} \right)^2 \right)} \right) + \tanh \left(a \sqrt{\mu_n \left(1 - \left(\frac{\xi_{n,j}}{c_-} \right)^2 \right)} \right) = 0. \quad (25)$$

for $\xi_{n,j} = \sqrt{\lambda_{n,j}/\mu_n} \in (-\infty, c_-)$, which it is impossible as the arguments of the hyperbolic tangents are strictly positive.

To distinguish the eigenpairs $\{(\lambda_{n,j}, w_{n,j})\}_{n,j \in \mathbb{N}}$ which correspond to interior modes from those ones which are associated with Love modes, for each index $n \in \mathbb{N}$, which fixes the mode q_n with the x_1 -dependency, the corresponding indexes $j \in \mathbb{N}$ are split in two disjoint sorted subsets: those

$w_{n,j}$ with $j \in I_n \subset \mathbb{N}$ are considered interior modes whereas if $j \in \mathcal{L}_n \subset \mathbb{N}$ then they are Love modes. The ordering of subsets \mathcal{L}_n and I_n are given by the natural ascending order with respect to the magnitude of their associated eigenvalues $\lambda_{n,j}$.

Remark 1. *Despite the spectral problems with $\beta = 0$ and $\beta > 0$ share similar variational formulations, the change of nature on the boundary condition type (from Robin to Neumann boundary condition on $\Gamma_e \cup \Gamma_s$) implies that the eigenfunctions of the auxiliary spectral problem (7)-(10) are not eigenfunctions of the spectral problem associated with the target problem (1)-(5). Moreover, even in the case of constant functions, it is straightforward to show that the spectral problem associated with (1)-(5) for $\beta > 0$ does not admit eigenfunctions of type $w(x_1, x_2) = p(x_2)$, since the non-null constant functions do not satisfy the Robin condition (3).*

4. Modal-based PUFEM method

The main idea of the proposed PUFEM methodology consists in the use of the information of the eigenmodes computed from an auxiliary spectral problem to be combined with a standard piecewise polynomial finite element discretization. Typically, any PUFEM discretization applied to a two-dimensional problem would involve a triangular or quadrilateral mesh of the computational domain. However, due to the tensor product representation and the assumptions (H1)-(H2) required to the computational domain (tangent to the coupling interface), the partition of unity can be settled only in one spatial coordinate direction, reducing the number of degrees of freedom used in the discretization and simultaneously keeping the information of the coupling phenomena of the layered material, which is already included in the computation of the eigenmodes.

4.1. Discrete space

Before the detailed description of the modal-based PUFEM discrete space, a preliminary analysis must be performed on the eigenmodes computed in Section 3. Firstly, those redundant eigenmodes which belong to the polynomial discrete finite element space should be removed from the PUFEM modal basis. In the particular case analysed in Section 3, q_0 is a constant function, so it belongs to the standard piecewise linear polynomial finite element space in the x_1 -coordinate. Its inclusion in the PUFEM discrete space does not add any new feature to the classical discrete FEM approximation, so it will be neglected from the discrete space.

Regarding the rest of eigenfunctions ($n > 0$), if expressions $q_n(x_1)$ were used directly to define the enrichment of the PUFEM discrete space, since the eigenmodes $w_{n,j}$ satisfy homogeneous Neumann boundary conditions on $\Gamma_e \cup \Gamma_s$, a lack of convergence will arise around the boundaries where the Robin conditions are considered in the target problem (1)-(5). To avoid this drawback, q_n is rewritten in terms of complex exponential of different sign,

$$q_n(x_1) = \sqrt{\frac{2}{L}} \left(\frac{1}{2} q_n^+(x_1) + \frac{1}{2} q_n^-(x_1) \right), \quad n \in \mathbb{N}, n \neq 0,$$

where $q_n^+(x_1) = \exp(i\sqrt{\mu_n}x_1)$ and $q_n^-(x_1) = \exp(-i\sqrt{\mu_n}x_1)$. Taking into account this new rewriting of the modes q_n using complex exponential expressions, if both functions q_n^+ and q_n^- are involved separately in the PUFEM discrete basis, it is guaranteed that any boundary condition on $\Gamma_e \cup \Gamma_s$ (located at $x_1 = 0$ and $x_1 = L$) could be satisfied by a linear combination of type $C_0 q_n^+ + C_1 q_n^-$ with adequate constants C_0 and C_1 .

Obviously, as it has been already discussed in the section above, for each $n \in \mathbb{N}$, the eigenmodes $w_{n,j}$, $j \in I_n$, associated with the interior modes are infinite (but countable) and for discretization purposes, this set of modes I_n must be truncated only considering a finite number of eigenmodes with the smallest magnitude. The truncated finite set of indexes for the interior modes will be denoted by $\tilde{I}_n \subset I_n$, being J_n the number of interior modes used in the discretization. The criterion to truncate the infinite sequence of interior modes corresponds to keep in the discretization only those interior eigenvalues $\lambda_{n,j}$ which satisfy

$$c_+^2 \mu_n \leq \lambda_{n,j} \leq c_0^2 \mu_n \quad \text{for } n = 0, \dots, N, \quad (26)$$

and where c_0 is the maximum value allowed for the solutions $\zeta_{n,j}$ of the dispersion equation (23). In the case of the eigenpairs associated with the Love modes, its dispersion equation only admits a finite number of solutions and so, for a fixed value $n \in \mathbb{N}$, all the Love eigenmodes are considered in the discretization. The number of Love eigenmodes included in the subset \mathcal{L}_n will be denoted by L_n . Using this notation, if $\lambda_{n,j}$ is an eigenvalue of the auxiliary spectral problem and its corresponding eigenmode is used in the PUFEM discretization, then there exists a k -th family of eigenmodes such that the pair of indexes $(n, j) \in \mathcal{J}^N = \{\{k\} \times (\mathcal{L}_k \cup \tilde{I}_k)\}_{k=1}^N$, or equivalently

$$n \in \{1, 2, \dots, N\} \quad \text{and} \quad j \in \underbrace{\{1, \dots, L_n\}}_{j \in \mathcal{L}_n} \cup \underbrace{\{L_n + 1, \dots, L_n + J_n\}}_{j \in \tilde{I}_n}. \quad (27)$$

To describe precisely the proposed modal-based PUFEM method, an one-dimensional finite element mesh must be introduced. For simplicity, an uniform mesh of size h will be used throughout the rest of the present work, this is, a mesh with M elements and whose nodes are given by $\{y_m = hm : m = 0, \dots, M\} \subset [0, L]$. Clearly, such mesh has $M + 1$ nodes and a mesh size $h = L/M$. In addition, the partition of unity consists in the local polynomial basis $\{\varphi_m\}_{m=0}^M$, which is the standard Lagrange \mathbb{P}_1 (piecewise linear) finite element basis, defined by the nodal relation $\varphi_m(y_l) = \delta_{lm}$, where δ_{lm} is the Kronecker's delta. Hence, the discrete modal-based PUFEM space \mathbf{X}_h is defined by the span of a tensor product basis as follows:

$$\mathbf{X}_h = \left\langle \left\{ (\varphi_m q_n^+) \otimes p_{n,j}, (\varphi_m q_n^-) \otimes p_{n,j}, m = 0, \dots, M, (n, j) \in \mathcal{J}^N \right\} \right\rangle, \quad (28)$$

where recall that $[(\varphi_m q_n^\pm) \otimes p_{n,j}](x_1, x_2) = \varphi_m(x_1) q_n^\pm(x_1) p_{n,j}(x_2)$ and the ordering of indexes (n, j) in the subsets \mathcal{L}_k and \tilde{I}_k are given by the natural ascending order with respect to the magnitude of their associated eigenvalues $\lambda_{n,j}$.

From the definition of \mathbf{X}_h and since $\{\varphi_m\}_{m=0}^M$ is a partition of unity of the interval $[0, L]$, i.e., $\sum_{m=0}^M \varphi_m(x_1) = 1$, it is clearly deduced that

$$w_{n,j} = \sqrt{\frac{1}{2L}} \sum_{m=0}^M (\varphi_m q_n^+ + \varphi_m q_n^-) \otimes p_{n,j} \in \mathbf{X}_h,$$

with $(n, j) \in \mathcal{J}^N$. hence, the proposed discretization inherits potentially the spectral convergence of the modal basis approximations (see Section 5 for the illustration of the numerical behaviour of the proposed method). Simultaneously, due to the use of a partition of unity, the functions used for the enrichment in the discrete space has not to satisfy all the boundary conditions of the

source problem, what increases the flexibility of choice for the modal basis. In addition, taking into account to the compact support of the finite element basis $\{\varphi_m\}_{m=0}^M$, the matrix of the discrete problem will be sparse, what decreases the computational storage requirements for a typical modal discretization which involves full discrete matrices.

Since the modal-based PUFEM enrichment is flexible enough to select only a part of the spectral basis, the impact in the accuracy of considering only Love modes in the discrete space has been analysed in the numerical results shown in Section 5. In this case, the discrete space is defined by

$$\mathbf{X}_h^{\mathcal{L}} = \left\langle \left\{ (\varphi_m q_n^+) \otimes p_{n,j}, (\varphi_m q_n^-) \otimes p_{n,j}, m = 0, \dots, M, (n, j) \in \mathcal{J}^N \right\} \right\rangle. \quad (29)$$

The numerical features of the proposed modal-based PUFEM discretization with these two discrete spaces are described in detail in the following two sections.

4.2. Matrix description of the discrete problem

To write the matrix description of the variational problem using the discrete space \mathbf{X}_h (and analogously $\mathbf{X}_h^{\mathcal{L}}$), each term of the variational formulation associated with the sesquilinear form A_β , the L^2 -inner product, the source, and the boundary data contributions (see (6)) are computed for unknown and test functions belonging to the discrete space. Hence, the discrete variational formulation can be stated as follows: For a fixed frequency $\omega > 0$, find $u_h \in \mathbf{X}_h$ such that

$$A_\beta(u_h, v_h) - \omega^2 \langle u_h, v_h \rangle_{L^2(\Omega)} = \ell(v_h) \quad \text{for all } v_h \in \mathbf{X}_h. \quad (30)$$

Clearly, any function $u_h \in \mathbf{X}_h$ is determined by their respective discrete vector

$$\begin{aligned} \vec{u}_h &= (((u_{mnj}^+, u_{mnj}^-)_{j \in \mathcal{L}_n \cup \tilde{\mathcal{I}}_n})_{m=0}^M)_{n=1}^N \\ &= (u_{011}^+, u_{011}^-, u_{012}^+, u_{012}^-, \dots, u_{01L_1+J_1}^+, u_{01L_1+J_1}^-, \dots, \\ &\quad u_{0NL_N+J_N}^+, u_{0NL_N+J_N}^-, u_{111}^+, u_{111}^-, \dots, u_{MNL_N+J_N}^+, u_{MNL_N+J_N}^-), \end{aligned} \quad (31)$$

and so the vector coefficients define the discrete function, this is,

$$u_h = \sum_{m=0}^M \sum_{n=1}^N \sum_{j=1}^{L_n+J_n} \left(u_{mnj}^+ (\varphi_m q_n^+) \otimes p_{n,j} + u_{mnj}^- (\varphi_m q_n^-) \otimes p_{n,j} \right). \quad (32)$$

The coefficient ordering in (31) has been chosen to reduce as much as possible the bandwidth of the sparse matrices involved in the discretization. In fact, since the degrees of freedom related to the same finite element basis φ_m are stored consecutively, it is straightforward to show that due to the compact support of the one-dimensional finite element basis, the bandwidth of the matrix description is given by $6 \max_{1 \leq n \leq N} (L_n + J_n)$.

Taking into account this basis representation in \mathbf{X}_h , the discrete variational formulation (30) admits the matrix description

$$-\omega^2 \mathcal{M} \vec{u}_h - i\omega\beta C \vec{u}_h + \mathcal{K} \vec{u}_h = \vec{b}_h, \quad (33)$$

where the coefficients of the matrices \mathcal{M} , C , and \mathcal{K} (with respect to the coordinates u_{mnj}^\pm , induced by the basis of \mathbf{X}_h) are given by the expressions written below. Taking into account the expression

of the sesquilinear form (6) and the discrete problem (30), the mass matrix \mathcal{M} is defined by

$$[\mathcal{M}]_{mnj,lki}^{\pm\mp} = \int_{\Omega} (\varphi_m q_n^{\pm}) \otimes p_{n,j} \overline{(\varphi_l q_k^{\mp})} \otimes p_{k,i} \, d\mathbf{x} = \left(\int_0^L \varphi_m \varphi_l q_n^{\pm} q_k^{\mp} \, dx_1 \right) \left(\int_{-a}^H p_{n,j} p_{k,i} \, dx_2 \right),$$

the damping matrix \mathcal{C} is given by

$$\begin{aligned} [\mathcal{C}]_{mnj,lki}^{\pm\mp} &= \int_{\Gamma_e \cup \Gamma_s} c (\varphi_m q_n^{\pm}) \otimes p_{n,j} \overline{(\varphi_l q_k^{\mp})} \otimes p_{k,i} \, d\sigma \\ &= \left((\varphi_m \varphi_l q_n^{\pm} q_k^{\mp})|_{x_1=0} + (\varphi_m \varphi_l q_n^{\pm} q_k^{\mp})|_{x_1=L} \right) \left(\int_{-a}^H p_{n,j} p_{k,i} \, dx_2 \right), \end{aligned}$$

and the stiffness matrix \mathcal{K} is defined by

$$\begin{aligned} [\mathcal{K}]_{mnj,lki}^{\pm\mp} &= \int_{\Omega} c^2 \int_{\Omega} \nabla((\varphi_m q_n^{\pm}) \otimes p_{n,j}) \cdot \nabla(\overline{(\varphi_l q_k^{\mp})} \otimes p_{k,i}) \, d\mathbf{x} \\ &= \left(\int_0^L (\varphi_m q_n^{\pm})' (q_k^{\mp} \varphi_l)' \, dx_1 \right) \left(\int_{-a}^H p_{n,j} p_{k,i} \, dx_2 \right) + \left(\int_0^L \varphi_m q_n^{\pm} q_k^{\mp} \varphi_l \, dx_1 \right) \left(\int_{-a}^H p'_{n,j} p'_{k,i} \, dx_2 \right), \end{aligned}$$

for all $0 \leq m, l \leq M$ and $(m, j), (k, i) \in \mathcal{J}^N$. It should be noted that all the integrals stated below have been computed using one-dimensional exact integration with closed form integral formulas (without requiring the use of quadrature formulas). Since the source and boundary terms, functions f , g , and r have been approximated by high-order polynomials (in the case of the source term, such interpolation has been performed assuming a tensor product expression), then the same exact quadrature procedure has been also applied to the right-hand side term \vec{b}_h . Consequently, the right-hand side in the linear system (33) is given by

$$\begin{aligned} [\vec{b}_h]_{mnj}^{\pm} &= \int_{\Omega} f(\varphi_m q_n^{\pm}) \otimes p_{n,j} \, d\mathbf{x} + \int_{\Gamma_+ \cup \Gamma_-} g(\varphi_m q_n^{\pm}) \otimes p_{n,j} \, d\sigma + \int_{\Gamma_e \cup \Gamma_s} c r(\varphi_m q_n^{\pm}) \otimes p_{n,j} \, d\sigma \\ &= \left(\int_0^L f_1 \varphi_m q_n^{\pm} \, dx_1 \right) \left(\int_{-a}^H f_2 p_{n,j} \, dx_2 \right) + p_{n,j}(-a) \int_0^L g|_{x_2=-a} \varphi_m q_n^{\pm} \, dx_1 \\ &\quad + p_{n,j}(H) \int_0^L g|_{x_2=H} \varphi_m q_n^{\pm} \, dx_1 + (\varphi_m q_n^{\pm})|_{x_1=0} \int_{-a}^H c r|_{x_1=0} p_{n,j} \, dx_2 \\ &\quad + (\varphi_m q_n^{\pm})|_{x_1=L} \int_{-a}^H c r|_{x_1=L} p_{n,j} \, dx_2, \end{aligned}$$

for all $0 \leq m \leq M$ and $(m, j) \in \mathcal{J}^N$. Obviously, from the symmetric character of the L^2 -inner product and the sesquilinear form A_{β} for $\beta = 0$, both matrices \mathcal{M} and \mathcal{K} are hermitian. A direct inspection on the coefficients of the damping matrix \mathcal{C} also reveals it is hermitian.

4.3. Analysis of the condition number

It is well known that the enriched methods and, in particular, those ones which are based on a partition of unity and plane waves suffer from a poor conditioning (see [3, 23] for a detailed description of effects of the conditioning on the PUFEM numerical results). The proposed modal-based partition of unity method also shares this kind of conditioning drawbacks even if the PUFEM discretization is restricted to a one-dimensional discretization in the x_1 -axis.

To check the origin of these conditioning issues, the condition number $\kappa(\mathcal{M})$ of the mass matrix \mathcal{M} will be analysed in a simplified case, where it has been considered the pure Neumann problem (with $\beta = 0$) for an one-layer material (i.e. $c^+ = c^-$) in the target problem (1)-(5). Similar arguments could be also applied to the stiffness and damping matrix \mathcal{K} and \mathcal{C} in the linear system (33). To highlight the different order of magnitude of conditioning in the proposed modal-based PUFEM method, it will be compared with those condition numbers coming from an standard finite element discretization.

First, notice that the condition number of the mass matrix is not an issue in a standard piecewise linear finite element discretization (in one-dimension with a uniform mesh). In this case, for the finite element mass matrix, its condition number is upper bounded independently of the mesh size h , this is, $\kappa(\mathcal{M}) = O(1)$ (see [10] for further details). In what follows, it will be checked that the condition number of the modal-based PUFEM mass matrix increases when the number of eigenmodes is enlarged and simultaneously a refined finite element mesh is used in the partition of unity). In fact, it will be shown that $\kappa(\mathcal{M}) = O(h^{-2})$.

Firstly, in the simple case of $\beta = 0$ and $c^- = c^+$, the modal basis solution of the spectral problem is given by $w_{n,j} = q_n \otimes p_j$, where recall that q_n , $n \in \mathbb{N}$, $n \neq 0$ are defined by (12) and p_j , $j \in \mathbb{N}$ are given as follows:

$$p_0(x_2) = \sqrt{\frac{1}{a+H}}, \quad p_j(x_2) = \sqrt{\frac{2}{a+H}} \cos\left(\frac{j\pi x_2}{a+H}\right), \quad j \in \mathbb{N}, j \neq 0.$$

Notice that $\{p_j\}_{j \in \mathbb{N}}$ is an orthonormal Hilbert basis in $L^2(-a, H)$. Following an analogous strategy to that one used to obtain (28), the discretization space X_h is defined by

$$X_h = \left\langle \left\{ (\varphi_m q_n^+) \otimes p_j, (\varphi_m q_n^-) \otimes p_j, \quad m = 0, \dots, M, \quad n, j = 0, \dots, N, \quad n \neq 0 \right\} \right\rangle, \quad (34)$$

where the Hilbert basis has been truncated to the first N eigenvalues. Hence, the complex-valued mass matrix \mathcal{M} of size $2N(N+1)(M+1) \times 2N(N+1)(M+1)$ inherits the tensor product description used in X_h , and after a reordering (permutation of rows and columns), it can be written as a Kronecker product of matrices $\mathcal{M} = \mathcal{A} \otimes \mathcal{B}$ (where the size of \mathcal{A} is $2(M+1)N \times 2(M+1)N$ and the size of \mathcal{B} is $(N+1) \times (N+1)$) being

$$[\mathcal{A}]_{mn, lk}^{\pm\mp} = \int_0^L \varphi_m \varphi_l q_n^\pm q_k^\mp dx_1, \quad \text{for } 0 \leq m, l \leq M, \quad 1 \leq n, k \leq N, \quad (35)$$

and

$$[\mathcal{B}]_{i,j} = \int_{-a}^H p_j p_i dx_2 \quad \text{for } 0 \leq i, j \leq N.$$

Trivially, from the orthogonality of the basis $\{p_j\}_{j \in \mathbb{N}}$, it is obtained that \mathcal{B} is the identity matrix I . Hence, in the simple case considered here, $\mathcal{M} = \mathcal{A} \otimes I$. Classical linear algebra results show that the spectrum of \mathcal{M} and \mathcal{A} coincides (see [18]) and so their condition number also coincides.

Lemma 1. *Let \mathcal{A} be the matrix defined by (35). If the finite element mesh satisfies $2(N+1) < M$ then it holds*

$$\kappa(\mathcal{A}) \geq Ch^{-2}, \quad (36)$$

where C is a positive constant independent of M and N , only dependent on L .

Proof. With the aim of estimating $\kappa(\mathcal{A})$, the numerical range of \mathcal{A} will be upper and lower bounded. Firstly, values m and n are fixed taking into account that $0 \leq m \leq M$ and $0 \leq n \leq N$. Then, consider the vector $\vec{v} \in \mathbb{C}^{2(M+1)N}$ associated with the discrete function $v \otimes p_n \in \mathbf{X}_h$ with $v(x_1) = \Phi_m(x_1) \sin(n\pi(x_1 - mh)/L)$, which corresponds to the following linear combination of basis functions:

$$v = \frac{\Phi_m}{2i} \left(\frac{q_n^+}{q_n^+(mh)} - \frac{q_n^-}{q_n^-(mh)} \right). \quad (37)$$

It holds

$$\begin{aligned} \vec{v}^* \mathcal{A} \vec{v} &= \int_0^L v(x_1) \bar{v}(x_1) dx_1 = \int_0^L \Phi_m^2(x_1) \sin^2 \left(\frac{n\pi(x_1 - mh)}{L} \right) dx_1 \\ &= 2 \int_0^h \frac{s^2}{h^2} \sin^2 \left(\frac{n\pi s}{L} \right) ds \leq C \int_0^h \frac{s^4}{h^2} ds \leq Ch^3, \end{aligned}$$

where each occurrence of constant C could denote a different value independent of h (only dependent on the ratio L/n). To obtain the estimate above, it has been used the first order Taylor polynomial approximation of the sine function around the origin. Now, it is straightforward to show from (37) that the unique non-null coefficients of \vec{v} are given by $(1/(2iq_n^+(mh)), -1/(2iq_n^-(mh)))$ and hence

$$\vec{v}^* \vec{v} = \left| \frac{1}{2i} e^{-i\frac{n\pi}{L}mh} \right|^2 + \left| \frac{1}{2i} e^{+i\frac{n\pi}{L}mh} \right|^2 = \frac{1}{2}, \quad (38)$$

and consequently, it has been shown that there exists $\vec{v} \neq \vec{0}$ such that

$$\frac{\vec{v}^* \mathcal{A} \vec{v}}{\vec{v}^* \vec{v}} \leq 2Ch^3.$$

Secondly, a different vector coordinate \vec{v} is taken into account. In this case, once m and n are fixed with $0 \leq m \leq M$ and $0 \leq n \leq N$, consider the vector $\vec{v} \in \mathbb{C}^{2(M+1)N}$ associated with the discrete function $v \otimes p_n \in \mathbf{X}_h$ with $v(x_1) = \Phi_m(x_1) \cos(n\pi(x_1 - mh)/L)$, which corresponds to the following linear combination of basis functions:

$$v = \frac{\Phi_m}{2} \left(\frac{q_n^+}{q_n^+(mh)} + \frac{q_n^-}{q_n^-(mh)} \right). \quad (39)$$

It holds

$$\begin{aligned} \vec{v}^* \mathcal{A} \vec{v} &= \int_0^L v(x_1) \bar{v}(x_1) dx_1 = \int_0^L \Phi_m^2(x_1) \cos^2 \left(\frac{n\pi(x_1 - mh)}{L} \right) dx_1 \\ &= 2 \int_0^h \frac{s^2}{h^2} \cos^2 \left(\frac{n\pi s}{L} \right) ds \geq \tilde{C} \int_0^h \frac{s^2}{h^2} ds \geq \tilde{C}h, \end{aligned} \quad (40)$$

where each occurrence of constant \tilde{C} could denote a different value independent of h (only dependent on the ratio L/n). To obtain the estimate above, it has been used a strictly positive lower bound for the cosine function in the compact interval $[0, h] \subset [0, L/(2(n+1))]$, which holds by assuming $2(n+1) > M$ and taking into account $h = L/M$. In the interval written above, it is ensured that

$\cos(n\pi s/L)$ is strictly positive for any n). Now, it is straightforward to show from (39) that the unique non-null coefficients of \vec{v} are given by $(1/(2q_n^+(mh)), 1/(2q_n^-(mh)))$ and hence, using (38), $\vec{v}^* \vec{v} = 1/2$. So, it has been shown that there exists $\vec{v} \neq \vec{0}$ such that

$$\frac{\vec{v}^* \mathcal{A} \vec{v}}{\vec{v}^* \vec{v}} \geq 2\tilde{C}h. \quad (41)$$

Now, if λ_{\max} and λ_{\min} are respectively the largest and smallest eigenvalues of matrix \mathcal{A} , using the classical property of the Rayleigh quotient for hermitian complex-valued matrices (which ensures that the numerical range is a real interval with eigenvalues as endpoints [27]), it holds

$$\lambda_{\min} \leq \frac{\vec{v}^* \mathcal{A} \vec{v}}{\vec{v}^* \vec{v}} \leq \lambda_{\max} \quad \text{for all } \vec{v} \neq \vec{0}.$$

Then, from (41) and (40), there exist two positive constants C and \tilde{C} , independent of M and N (and hence also independent of h) such that

$$2\tilde{C}h \leq \lambda_{\max} \quad \text{and} \quad \lambda_{\min} \leq 2Ch^3.$$

Consequently, since \mathcal{A} is a positive definite hermitian matrix (it is associated with the L^2 -inner product in X_h), it is satisfied

$$\kappa(\mathcal{A}) = \frac{\lambda_{\max}}{\lambda_{\min}} \geq \frac{\tilde{C}}{C}h^{-2}, \quad (42)$$

and hence (36) is obtained. \square

In conclusion, from Lemma 1, since the spectrum of \mathcal{A} and \mathcal{M} coincides, it is obtained that $\kappa(\mathcal{M}) = O(h^{-2})$, what implies a significant increasing of the condition number as soon as the finite element mesh is refined. This high condition number (compared with respect to the low conditioning of standard finite element methods) in the mass matrix could indicate the numerical mechanism because of the matrix of the linear system (33) suffers for high condition numbers. As it is reported in the following sections, to mitigate as much as possible the conditioning issues, different regularization techniques can be considered, the finite element meshes have been kept as coarse as possible in most of the numerical test, and also a novel criterion to limit the number of eigenmodes used in the discrete space has been derived.

5. Numerical results

An extensive variety of numerical tests has been considered to illustrate the performance and the numerical behaviour of the proposed modal-based PUFEM method. With this aim, different scenarios involving different discrete settings have been used. More precisely, Section 5.1 shows the different numerical performance obtained with a discrete space that only involves Love modes, and with another discrete space that includes both, Love and interior modes. Finally, in those numerical simulations where only interior modes are involved, the eigenmodes used in the modal-based PUFEM discretization (29) hold the condition (26) with $c_0 = 2c_+$.

Section 5.2 illustrates the consistency of the method for solutions contained in the discrete space, and Section 5.3 shows the accurate approximation of solutions which are close to the

constant-valued eigenmode (not included in the modal-based PUFEM discrete space (28)). Finally, Section 5.4 focuses on the deterioration of the numerical results due to the high condition numbers of the discrete matrix and its potential mitigation using regularization techniques.

Throughout the entire Section 5, the relative errors are computed using a pointwise L^∞ -norm on an 5×5 equispaced Cartesian grid of points $\{y_{jk}\}_{j,k=1}^5$ in the domain $[0, L] \times [-a, H]$. More precisely, the relative error is given by

$$\varepsilon_h = \frac{\max_{1 \leq j, k \leq 5} |u(y_{jk}) - u_h(y_{jk})|}{\max_{1 \leq j, k \leq 5} |u(y_{jk})|},$$

where u is the exact solution of the source problem and u_h is the approximated solution computed with the proposed modal-based PUFEM method. Other finer grids with a larger number of points have been also considered leading to similar relative errors. To plot the approximated solution computed by means of the modal-based PUFEM method, the real part of the approximation in every numerical test is plotted on a 17×17 equispaced grid of points $\{y_{jk}\}_{j,k=1}^{17}$ in the domain $[0, L] \times [-a, H]$. Additionally, the pointwise relative error with respect to L^∞ -norm is also plotted in the computational domain Ω .

If it is not mentioned explicitly other data, the numerical test have been computed assuming that problem (1)-(5) is settled with angular frequency $\omega = \pi$ and homogeneous Neumann boundary conditions have been considered on the whole boundary $\partial\Omega$. The computational domain $\Omega = (0, L) \times (-a, H)$ with $a = 0.2$, $H = 0.8$, $L = 1$ is split in two subdomains where the speed of sound is given by $c_- = 1/2$ in $\Omega_- = (0, L) \times (-a, 0)$ and $c_+ = 1$ in $\Omega_+ = (0, L) \times (0, H)$.

5.1. Numerical comparison of discrete spaces with or without interior modes

To illustrate the relevance of including the interior modes on the discrete space (and consequently use the complete set of eigenmodes computed from the auxiliary spectral problem), a detailed comparison between the modal-based method have being carried out using the discrete spaces X_h^L (only considering Love eigenmodes) and X_h (using Love and interior eigenmodes).

In this numerical test, the source term is given by

$$f(x_1, x_2) = \begin{cases} 1 & \text{for } (x_1, x_2) \in \Omega_+, \\ x_2 & \text{for } (x_1, x_2) \in \Omega_-, \end{cases}$$

and the boundary functions are fixed to $g = 0$ and $r = 0$. Assuming these boundary conditions and this source term, it is straightforward to compute the exact solution in closed form. More precisely, the exact solution is given by

$$u(x_1, x_2) = \begin{cases} A_+ e^{-i\omega x_2/c_+} + B_+ e^{i\omega x_2/c_+} - \frac{1}{\omega^2} & \text{if } (x_1, x_2) \in \Omega_+, \\ A_- e^{-i\omega x_2/c_-} + B_- e^{i\omega x_2/c_-} - \frac{x_2}{\omega^2} & \text{if } (x_1, x_2) \in \Omega_-, \end{cases} \quad (43)$$

being A_+, B_+, A_-, B_- coefficients that are determined by solving the linear system

$$\begin{pmatrix} 0 & 0 & e^{-i\omega H/c_+} & -e^{i\omega H/c_+} \\ e^{i\omega a/c_-} & -e^{-i\omega a/c_-} & 0 & 0 \\ 1 & 1 & -1 & -1 \\ 1 & -1 & -c_+/c_- & c_+/c_- \end{pmatrix} \begin{pmatrix} A_- \\ B_- \\ A_+ \\ B_+ \end{pmatrix} = \begin{pmatrix} 0 \\ ic_-/\omega^3 \\ -1/\omega^2 \\ ic_-/\omega^3 \end{pmatrix},$$

that results from applying the boundary conditions and the coupling conditions.

Table 1 shows the relative error for both, an approximated solution in the discrete space $X_h^{\mathcal{L}}$ involving only Love eigenmodes and an approximated solution in the discrete space X_h with Love and interior eigenmodes. As it is expected, if interior and Love modes are included in the discretization then the approximated PUFEM solutions are much more accurate than those computed with only Love modes. This conclusion is valid for any value of mesh size M and any number of eigenmodes N as it can be checked in Table 1. Figures 3 and 4 illustrate the real part of the approximated solution and the relative error for $M = 4$ and $N = 10$ computed using the discrete space $X_h^{\mathcal{L}}$ and X_h , respectively.

M	N	$X_h^{\mathcal{L}}$ (without interior modes)			X_h (with interior modes)		
		dof	ϵ_h	κ	dof	ϵ_h	κ
1	3	16	1.65×10^0	1.1×10^3	60	2.14×10^{-3}	1.5×10^8
	5	32	2.95×10^0	5.0×10^4	140	3.00×10^{-5}	3.1×10^{13}
	10	100	1.87×10^0	9.4×10^8	500	1.55×10^{-5}	1.2×10^{19}
4	3	40	3.53×10^0	1.0×10^5	150	7.28×10^{-5}	2.7×10^{12}
	5	80	4.45×10^{-1}	1.1×10^8	350	1.72×10^{-5}	5.2×10^{16}
	10	250	3.30×10^{-3}	1.3×10^{14}	1250	3.88×10^{-6}	1.0×10^{23}
10	3	88	5.17×10^0	3.5×10^8	330	2.73×10^{-5}	3.6×10^{15}
	5	176	6.62×10^{-2}	4.1×10^{11}	770	7.74×10^{-6}	2.0×10^{18}
	10	550	3.69×10^{-4}	6.2×10^{16}	2750	1.97×10^{-5}	2.2×10^{19}

Table 1: Comparison of the relative error ϵ_h and the condition number κ for two different approximated PUFEM solutions: the discrete space $X_h^{\mathcal{L}}$ that only includes Love modes (left part), and the discrete space X_h with both Love and interior eigenmodes (right part). The numerical results are shown for different values of the mesh size M , the number of eigenpair families considered in the discretization N , and the degrees of freedom (dof) of the discrete approximation.

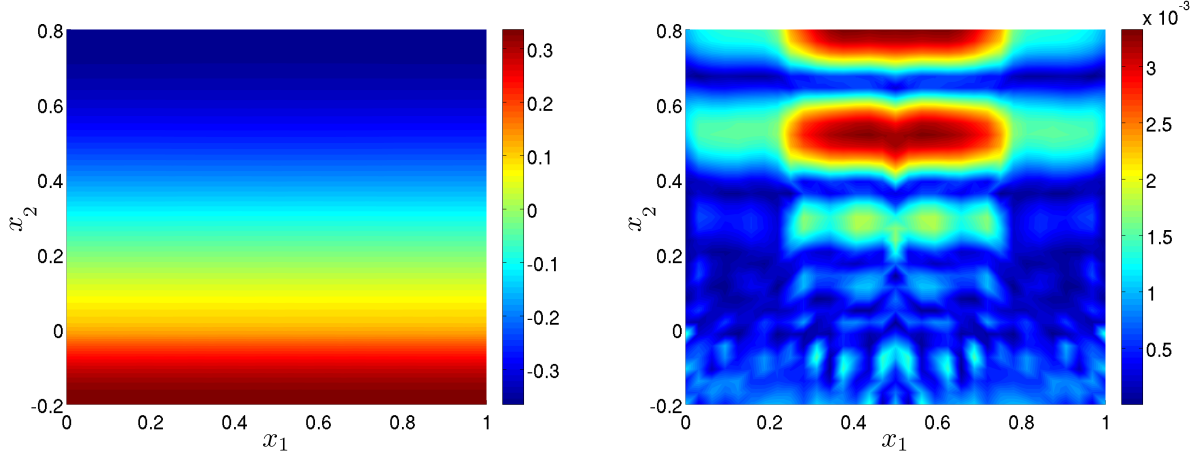


Figure 3: Real part of the approximated solution (left) and modulus of the relative error (right), obtained from the modal-based PUFEM method with a one-dimensional mesh of four elements (i.e. $M = 4$) and considering the discrete space $X_h^{\mathcal{L}}$ with $N = 10$. The exact solution is given by (43).

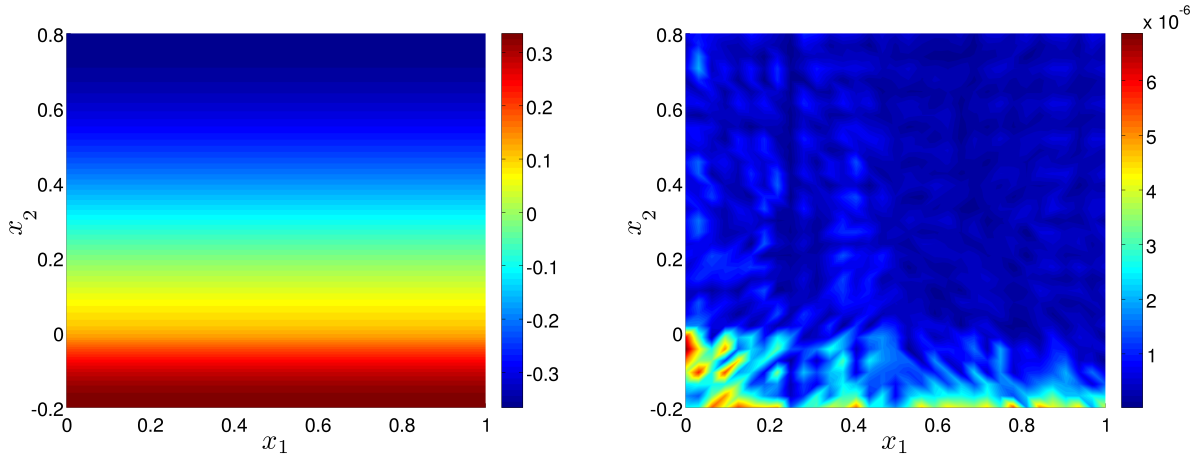


Figure 4: Real part of the approximate solution (left) and relative error (right), obtained from the modal-based PUFEM method with a one-dimensional mesh of four elements (i.e. $M = 4$) and considering the family of Love and interior modes $w_{n,j}$ with $(n, j) \in \{1, \dots, 10\} \times \{\mathcal{L}_n \cup I_n^j\}$ (i.e. $N = 10$). The exact solution is given by (43).

It is also relevant that, if the relative errors obtained with both discrete spaces are compared for similar values of degrees of freedom (and hence with almost similar computational cost), the numerical results reached with the discrete X_h outperforms those results obtained with only Love modes in $X_h^{\mathcal{L}}$. In conclusion, the numerical results described throughout the rest of this section, will take into account both Love and interior eigenmodes and hence the proposed modal-based PUFEM discretization will always use the discrete space X_h .

5.2. Consistency of the modal-based PUFEM method with Love and interior modes

In order to check the consistency of the modal-based PUFEM method (using the discrete space with both interior and Love modes), the relative error has been analysed in some numerical tests where the exact solutions belong to the discrete space X_h . It is shown here the case where the exact

solution is given by an interior mode. Numerical results obtained choosing a Love mode as exact solution are analogous to the ones shown in this section.

The solution considered in this test is the eigenmode associated with the lowest non-null eigenvalue, this is, $u = w_{1,L_1+1}$, where $(1, L_1 + 1) \in \mathcal{J}^N$ (see (27)). To obtain such exact solution, the source term is given by $f = (\lambda_{1,L_1+1} - \omega^2)w_{1,L_1+1}$. Obviously, from a theoretical point of view, since the exact solution belongs to the discrete space, the numerical approximation error should be null. However, due to the round-off errors introduced by the double precision arithmetic representation and the high condition number of the discrete matrices, the relative errors shown in the first two rows of Table 2 are reaching approximately $O(10^{-14})$. The numerical results of Table 2 also illustrate how the relative errors are increased as the one-dimensional mesh is refined (M is increased) and more eigenmodes are involved in the discrete space X_h (value of N is increased). In both cases, since the condition number of the linear system grows, the relative errors are also increased. Despite of this well-known phenomena for partition of unity methods, it should be remarked that five digits of accuracy are kept even in those numerical approximations where the condition number is as high as $O(10^{18})$. Figure 5 illustrates the real part of the approximated solution and the relative error for $M = 10$ and $N = 3$.

M	N	dof	ε_h	κ
1	1	12	1.49×10^{-15}	1.5×10^2
	3	60	3.81×10^{-14}	1.5×10^8
	5	140	6.60×10^{-12}	3.1×10^{13}
100	1	606	2.78×10^{-11}	2.5×10^{13}
	3	3030	1.06×10^{-5}	1.4×10^{18}
	5	7070	4.92×10^{-6}	9.5×10^{18}

Table 2: Relative error ε_h and the condition number κ for different values of the mesh size M , the number of eigenmodes N considered in the discretization, and the degrees of freedom (dof) used in the discrete approximation. The exact solution is given by the non-constant interior mode associated with the lowest eigenvalue.

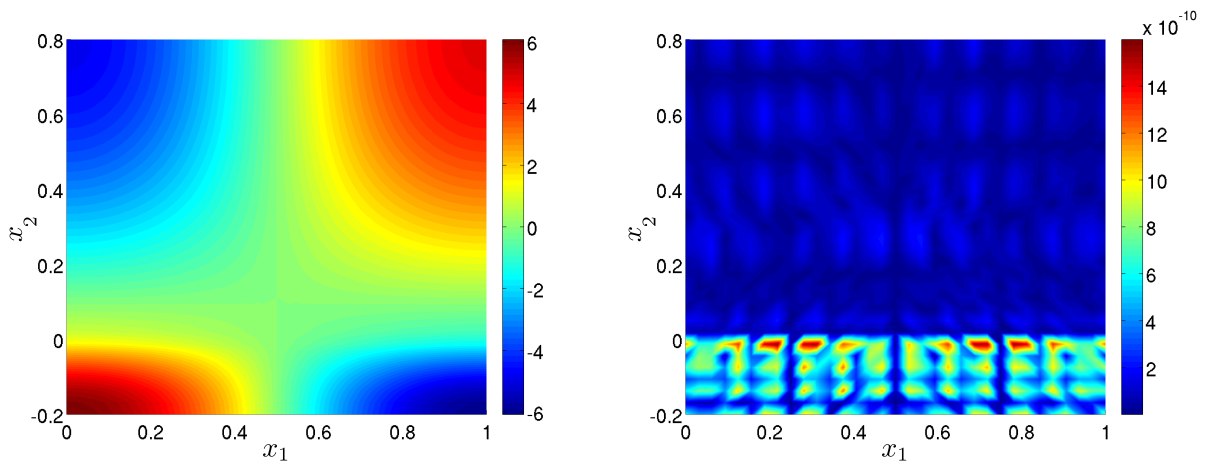


Figure 5: Real part of the approximated solution (left) and modulus of the relative error (right) obtained from the modal-based PUFEM method with a one-dimensional mesh of ten elements (i.e. $M = 10$) and considering the discrete space X_h with $N = 3$). The exact solution is the non-constant interior mode associated with the lowest eigenvalue.

5.3. Accurate approximation of eigenmodes not included in the discrete space

It has been discussed in previous sections that those eigenmodes corresponding to the constant factors $q_0(x_1)$ are not considered in the definition of the discrete space X_h . So, it could be natural to conclude that the exact solutions of the form $q_0 \otimes p$ in problem (1)-(5) could be inaccurately approximated by the modal-based PUFEM method. However, the numerical test described in this section illustrates the high accuracy of the method even in this scenario.

The source term has been fixed to $f = 1$ to obtain as exact solution $u = -1/\omega^2$. Table 3 shows that, even if the eigenmodes which are independent of the x_1 spatial coordinate are not included in the modal-based discretization, the constant exact solution can be approximated accurately with similar relative errors to those obtained in the approximation of solutions belonging to X_h (see the right part of Table 1).

M	N	dof	ε_h	κ
1	1	12	1.21×10^{-1}	1.5×10^2
	3	60	2.31×10^{-3}	1.5×10^8
	5	140	1.61×10^{-5}	3.1×10^{13}
100	1	606	9.38×10^{-3}	2.5×10^{13}
	3	3030	1.66×10^{-5}	1.4×10^{18}
	5	7070	1.26×10^{-5}	8.2×10^{18}

Table 3: Relative error ε_h and the condition number κ for different values of the mesh size M , the number of eigenmodes N considered in the discretization, and the degrees of freedom (dof) used in the discrete approximation. The exact solution is constant.

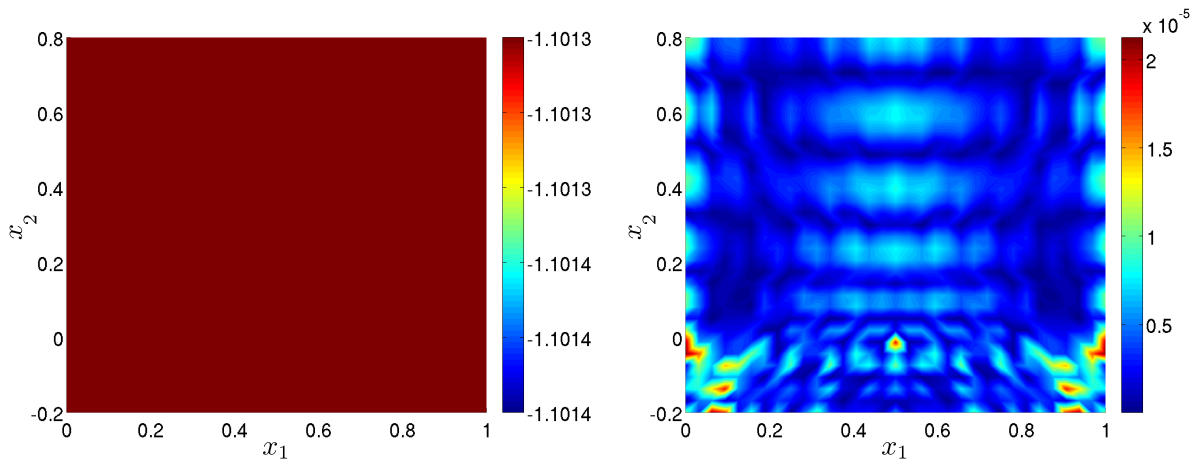


Figure 6: Real part of the approximated solution (left) and modulus of the relative error (right), obtained from the modal-based PUFEM method with a one-dimensional mesh of ten elements (i.e. $M = 10$) and considering the discrete space X_h with $N = 3$. The exact solution is constant.

5.4. Influence of the condition number on the numerical results

In previous sections, it has been reported that the modal-based PUFEM method suffers for large condition numbers in the linear systems which have to be solved. Such issue represents a potential drawback in the use of direct LU-based linear solvers. From the numerical results

described in the sections above and the theoretical analysis made in Section 4.3, this conditioning problem is more relevant as soon as the one-dimensional finite element mesh is refined and the number of eigenmodes involved in the discrete space is increased. However, there exists a number of methodologies to deal with high condition numbers and try to mitigate the amplification of the round-off errors on the solution of linear systems. Three different regularization techniques have been evaluated: a naive damping strategy, the classical Tikhonov filtering (with two different strategies to choose the regularization parameter), and the truncated singular value decomposition method. The latter has been already used for solving linear systems with large condition numbers in the context of two-dimensional PUFEM discretizations (see [6]).

Now, to avoid those exact solutions which could belong to X_h , the source term is given by

$$f(x_1, x_2) = \begin{cases} \cos\left(\frac{3\pi x_1}{L}\right) & \text{for } (x_1, x_2) \in \Omega_+, \\ (1+x_2)\cos\left(\frac{3\pi x_1}{L}\right) & \text{for } (x_1, x_2) \in \Omega_-. \end{cases}$$

With this source term, it is straightforward to compute the exact solution in closed form, which does not belong to X_h , and it is given by

$$u(x_1, x_2) = \cos\left(\frac{3\pi x_1}{L}\right) \begin{cases} A_+ e^{-i\alpha_+ x_2} + B_+ e^{i\alpha_+ x_2} - \frac{1}{c_+^2 \alpha_+^2} & \text{if } (x_1, x_2) \in \Omega_+, \\ A_- e^{-i\alpha_- x_2} + B_- e^{i\alpha_- x_2} - \frac{1+x_2}{c_-^2 \alpha_-^2} & \text{if } (x_1, x_2) \in \Omega_-, \end{cases} \quad (44)$$

where

$$\alpha_+ = \sqrt{\frac{\omega^2}{c_+^2} - \frac{9\pi^2}{L^2}}, \quad \alpha_- = \sqrt{\frac{\omega^2}{c_-^2} - \frac{9\pi^2}{L^2}},$$

and A_+ , B_+ , A_- , B_- are the coefficients computed as solution of the linear system

$$\begin{pmatrix} 0 & 0 & -e^{-i\alpha_+ H} & e^{i\alpha_+ H} \\ -i\alpha_- e^{i\alpha_- a} & i\alpha_- e^{-i\alpha_- a} & 0 & 0 \\ -1 & -1 & 1 & 1 \\ ic_-^2 \alpha_- & -ic_-^2 \alpha_- & -ic_+^2 \alpha_+ & ic_+^2 \alpha_+ \end{pmatrix} \begin{pmatrix} A_- \\ B_- \\ A_+ \\ B_+ \end{pmatrix} = \begin{pmatrix} 0 \\ 1/c_-^2 \alpha_-^2 \\ 1/c_+^2 \alpha_+^2 - 1/c_-^2 \alpha_-^2 \\ -1/\alpha_-^2 \end{pmatrix},$$

which results from applying the boundary conditions and the coupling conditions.

Firstly, Table 4 shows the comparison of the relative errors obtained with a LU-based direct solver and with the naive damping algorithm (adding a damping coefficient λ_d on the diagonal entries of the matrix). It can be observed that both methodologies lead to similar relative errors without any significant advantage between both methods. Analogous conclusions can be deduced from the numerical results reported for the truncated singular value decomposition (see Tables 7 and 8), and the Tikhonov filtering technique (see Tables 5, and 6), both in the case where the regularization parameter is chosen using either a L-curve strategy or the generalized cross validation (GCV) method.

M	N	dof	λ_d	ϵ_h	ϵ_d	κ
1	3	60	8.7×10^{-7}	1.13×10^{-3}	1.14×10^{-3}	1.5×10^8
	5	140	5.3×10^{-10}	1.24×10^{-4}	1.25×10^{-4}	3.1×10^{13}
	10	500	2.3×10^{-12}	1.05×10^{-4}	3.89×10^{-5}	1.2×10^{19}
4	3	150	2.8×10^{-7}	6.79×10^{-5}	8.33×10^{-5}	2.7×10^{12}
	5	350	2.3×10^{-10}	4.70×10^{-5}	6.61×10^{-5}	5.2×10^{16}
	10	1250	2.3×10^{-12}	4.70×10^{-5}	2.90×10^{-5}	3.9×10^{20}
10	3	330	3.8×10^{-9}	1.33×10^{-4}	1.22×10^{-4}	1.5×10^{15}
	5	770	1.0×10^{-12}	5.47×10^{-5}	5.71×10^{-5}	3.1×10^{18}
	10	2750	1.1×10^{-12}	4.94×10^{-5}	2.53×10^{-5}	1.2×10^{19}

Table 4: Comparison of the relative error ϵ_h computed from solving the discrete linear system using a LU-based direct solver and the relative error ϵ_d obtained using a naive damping method. The relative errors and the condition number κ are reported for different values of the mesh size M , the number of eigenmodes N considered in the discretization, and the degrees of freedom (dof) of the discrete approximation.

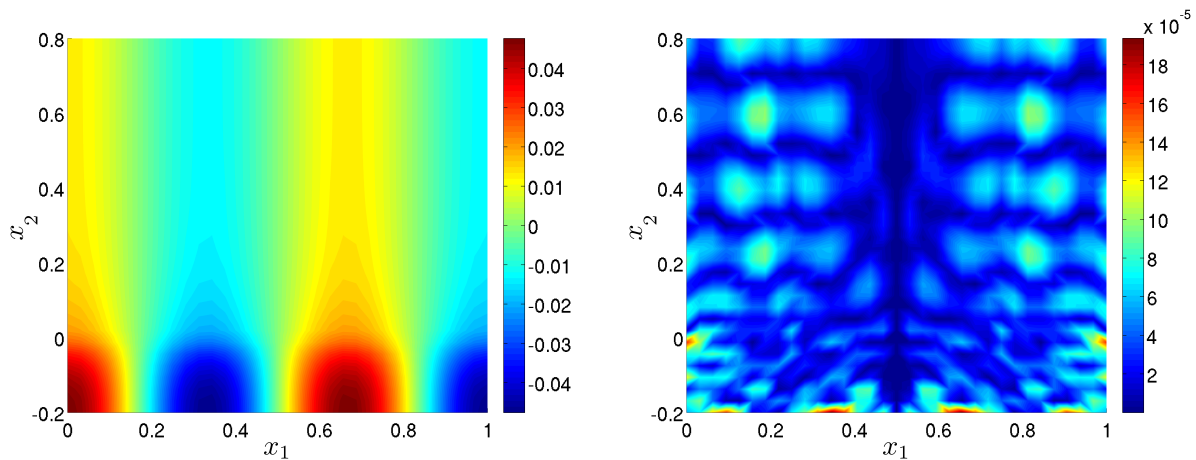


Figure 7: Real part of the approximate solution (using a LU-based direct solver) (left) and modulus of the relative error (right), obtained from the modal-based PUFEM method with a one-dimensional mesh of four elements (i.e. $M = 4$) and considering the discrete space X_h with $N = 3$. The exact solution is given by (44).

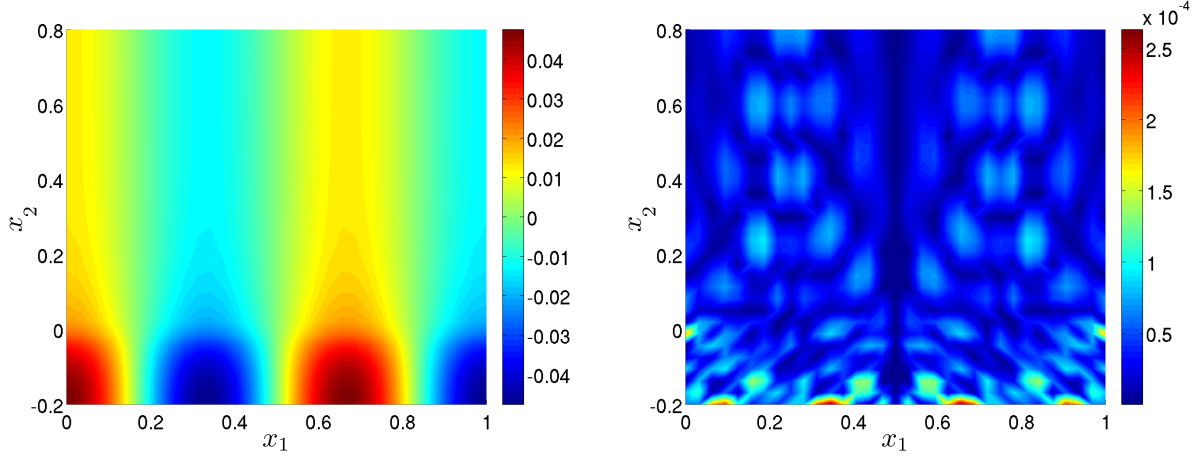


Figure 8: Real part of the approximate solution (using a naive damping method) (left) and modulus of the relative error (right), obtained from the modal-based PUFEM method with a one-dimensional mesh of four elements (i.e. $M = 4$) and considering the discrete space X_h with $N = 3$. The exact solution is given by (44).

M	N	dof	λ_t (L-curve)	ϵ_h	ϵ_t (L-curve)	κ
1	3	60	6.3×10^{-5}	1.13×10^{-3}	1.31×10^{-3}	1.5×10^8
	5	140	6.2×10^{-9}	1.24×10^{-4}	1.22×10^{-4}	3.1×10^{13}
	10	500	4.8×10^{-8}	1.05×10^{-4}	6.79×10^{-5}	1.2×10^{19}
4	3	150	3.6×10^{-6}	6.79×10^{-5}	6.79×10^{-5}	2.7×10^{12}
	5	350	2.0×10^{-9}	4.70×10^{-5}	4.70×10^{-5}	5.2×10^{16}
	10	1250	4.0×10^{-2}	4.70×10^{-5}	4.70×10^{-5}	3.9×10^{20}
10	3	330	7.9×10^{-5}	1.33×10^{-4}	1.33×10^{-4}	1.5×10^{15}
	5	770	2.6×10^{-11}	5.47×10^{-5}	5.47×10^{-5}	3.1×10^{18}
	10	2750	6.8×10^{-9}	4.94×10^{-5}	4.94×10^{-5}	1.2×10^{19}

Table 5: Comparison of the relative error ϵ_h computed from solving the discrete linear system using a LU-based direct solver and the relative error ϵ_t obtained by using the Tikhonov filtering technique (whose regularization parameter has been chosen by the L-curve). The relative errors and the condition number κ are reported for different values of the mesh size M , the number of eigenmodes N considered in the discretization, and the degrees of freedom (dof) of the discrete approximation.

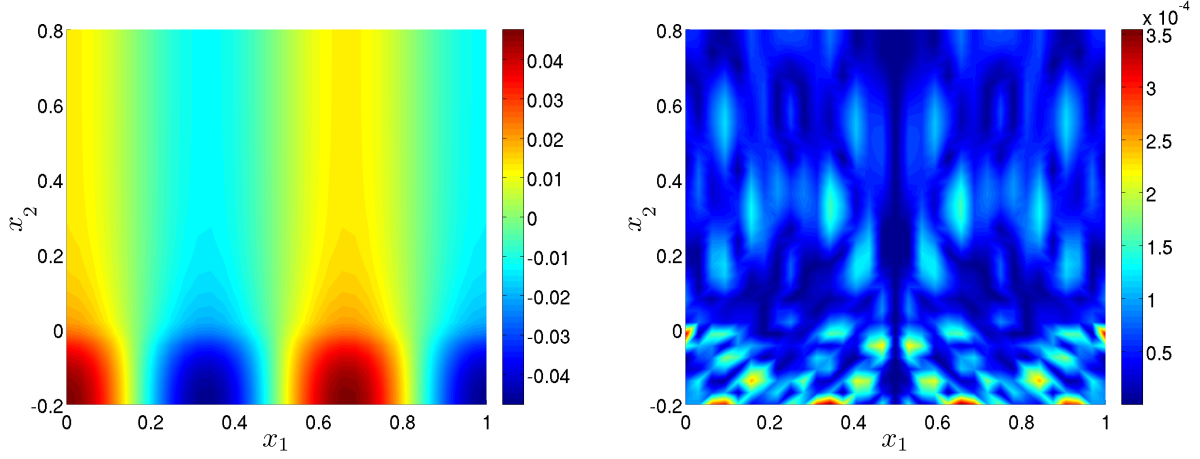


Figure 9: Real part of the approximate solution (using the Tikhonov filtering technique whose regularization parameter has been chosen by the L-curve) (left) and modulus of the relative error (right), obtained from the modal-based PUFEM method with a one-dimensional mesh of four elements (i.e. $M = 4$) and considering the discrete space X_h with $N = 3$. The exact solution is given by (44).

M	N	dof	λ_t (GCV)	ϵ_h	ϵ_t (GCV)	κ
1	3	60	9.2×10^{-5}	1.13×10^{-3}	1.24×10^{-3}	1.5×10^8
	5	140	2.2×10^{-10}	1.24×10^{-4}	1.25×10^{-4}	3.1×10^{13}
	10	500	1.8×10^{-10}	1.05×10^{-4}	4.54×10^{-5}	1.2×10^{19}
4	3	150	6.0×10^{-10}	6.79×10^{-5}	6.78×10^{-5}	2.7×10^{12}
	5	350	1.7×10^{-11}	4.70×10^{-5}	5.52×10^{-5}	5.2×10^{16}
	10	1250	1.3×10^{-10}	4.70×10^{-5}	3.49×10^{-5}	3.9×10^{20}
10	3	330	7.9×10^{-12}	1.33×10^{-4}	1.33×10^{-4}	1.5×10^{15}
	5	770	2.4×10^{-11}	5.47×10^{-5}	5.88×10^{-5}	3.1×10^{18}
	10	2750	8.1×10^{-11}	4.94×10^{-5}	2.74×10^{-5}	1.2×10^{19}

Table 6: Comparison of the relative error ϵ_h computed from solving the discrete linear system using a LU-based direct solver and the relative error ϵ_t obtained by using the Tikhonov filtering technique (whose regularization parameter has been chosen by the generalized cross validation technique). The relative errors and the condition number κ are reported for different values of the mesh size M , the number of eigenmodes N considered in the discretization, and the degrees of freedom (dof) of the discrete approximation.

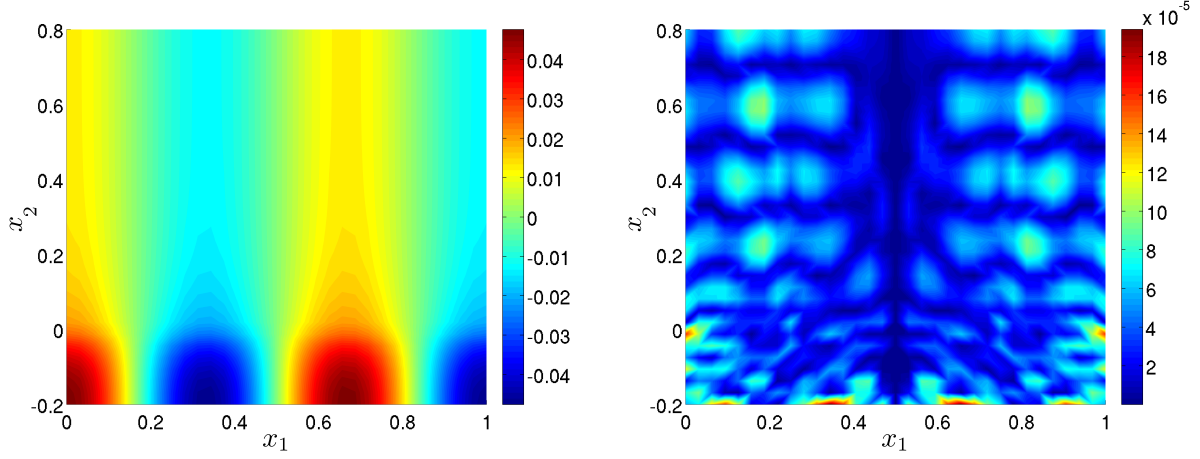


Figure 10: Real part of the approximate solution (using the Tikhonov filtering technique whose regularization parameter has been chosen by the generalized cross validation technique) (left) and modulus of the relative error (right), obtained from the modal-based PUFEM method with a one-dimensional mesh of four elements (i.e. $M = 4$) and considering the discrete space X_h with $N = 3$. The exact solution is given by (44).

M	N	dof	λ_{svd} (L-curve)	ϵ_h	ϵ_{svd} (L-curve)	κ
1	3	60	23	1.13×10^{-3}	1.53×10^{-1}	1.5×10^8
	5	140	119	1.24×10^{-4}	1.39×10^{-4}	3.1×10^{13}
	10	500	94	1.05×10^{-4}	8.94×10^{-1}	1.2×10^{19}
4	3	150	119	6.79×10^{-5}	8.94×10^{-4}	2.7×10^{12}
	5	350	94	4.70×10^{-5}	1.35×10^{-2}	5.2×10^{16}
	10	1250	538	4.70×10^{-5}	4.08×10^{-5}	3.9×10^{20}
10	3	330	39	1.33×10^{-4}	1.19×10^0	1.5×10^{15}
	5	770	678	5.47×10^{-5}	5.89×10^{-5}	3.1×10^{18}
	10	2750	568	4.94×10^{-5}	2.50×10^{-4}	1.2×10^{19}

Table 7: Comparison of the relative error ϵ_h computed from solving the discrete linear system using a LU-based direct solver and the relative error ϵ_{svd} obtained by using the truncated singular value decomposition method (whose regularization parameter has been chosen by the L-curve technique). The relative errors and the condition number κ are reported for different values of the mesh size M , the number of eigenmodes N considered in the discretization, and the degrees of freedom (dof) of the discrete approximation.

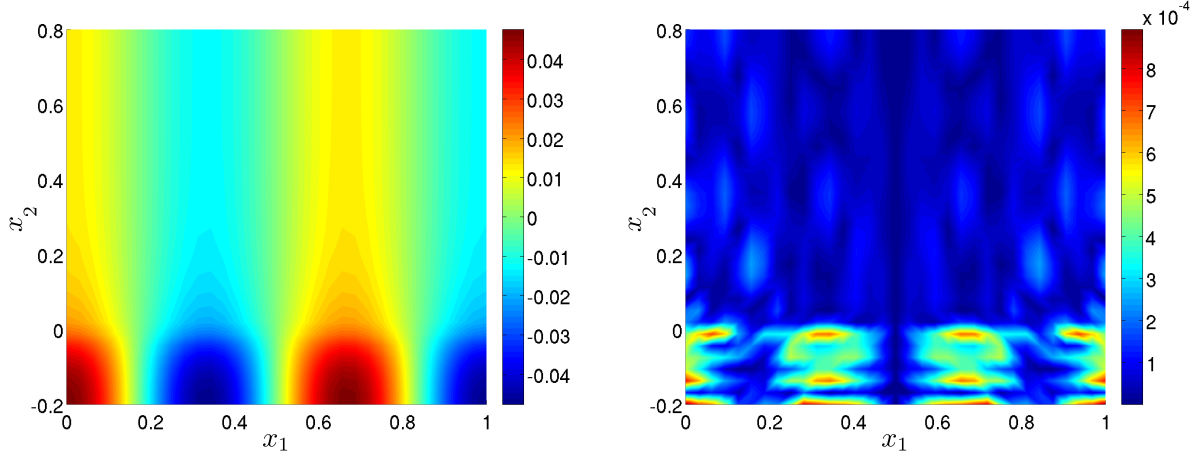


Figure 11: Real part of the approximate solution (using the truncated singular value decomposition method whose regularization parameter has been chosen by the L-curve technique) (left) and modulus of the relative error (right), obtained from the modal-based PUFEM method with a one-dimensional mesh of four elements (i.e. $M = 4$) and considering the discrete space X_h with $N = 3$. The exact solution is given by (44).

M	N	dof	λ_{svd} (GCV)	ϵ_h	ϵ_{svd} (GCV)	κ
1	3	60	59	1.13×10^{-3}	1.25×10^{-3}	1.5×10^8
	5	140	139	1.24×10^{-4}	1.24×10^{-4}	3.1×10^{13}
	10	500	468	1.05×10^{-4}	3.53×10^{-5}	1.2×10^{19}
4	3	150	149	6.79×10^{-5}	6.78×10^{-5}	2.7×10^{12}
	5	350	345	4.70×10^{-5}	5.06×10^{-5}	5.2×10^{16}
	10	1250	1017	4.70×10^{-5}	2.79×10^{-5}	3.9×10^{20}
10	3	330	327	1.33×10^{-4}	1.33×10^{-4}	1.5×10^{15}
	5	770	735	5.47×10^{-5}	5.73×10^{-5}	3.1×10^{18}
	10	2750	2500	4.94×10^{-5}	2.46×10^{-5}	1.2×10^{19}

Table 8: Comparison of the relative error ϵ_h computed from solving the discrete linear system using a LU-based direct solver and the relative error ϵ_{svd} obtained by using the truncated singular value decomposition method (whose regularization parameter has been chosen by the generalized cross validation technique). The relative errors and the condition number κ are reported for different values of the mesh size M , the number of eigenmodes N considered in the discretization, and the degrees of freedom (dof) of the discrete approximation.

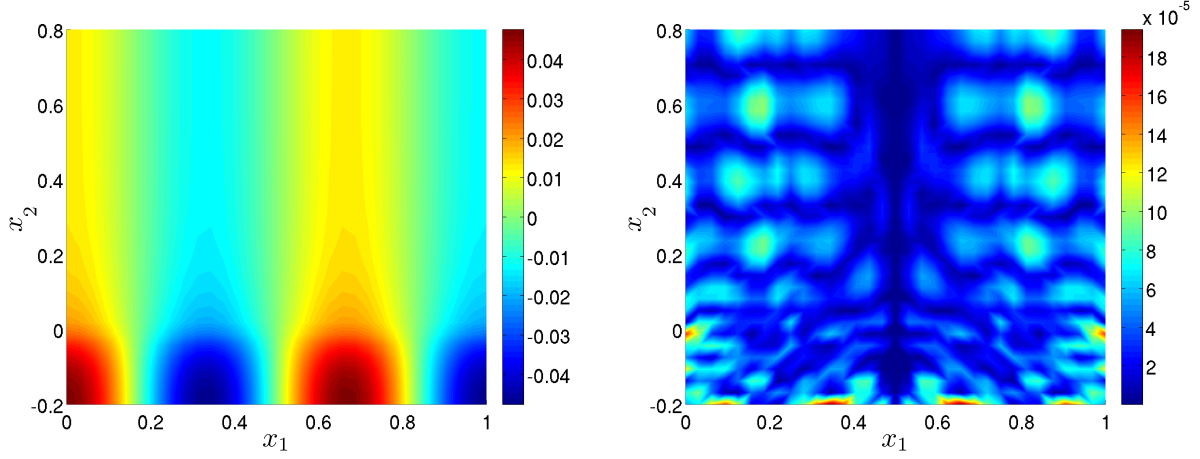


Figure 12: Real part of the approximate solution (using the truncated singular value decomposition method whose regularization parameter has been chosen by the generalized cross validation technique) (left) and modulus of the relative error (right), obtained from the modal-based PUFEM method with a one-dimensional mesh of four elements (i.e. $M = 4$) and considering the discrete space X_h with $N = 3$). The exact solution is given by (44).

6. PUFEM basis criterion based on the crack observability

The effect of the mesh and the choice of an adequate basis is essential to obtain accurate and reliable numerical results in any PUFEM technique due to the high condition number of the assembled matrices to be solved. Despite the recommendation of using coarse meshes to define the partition of unity, it is possible to design other criteria for selecting the most relevant eigenmodes involved in the definition of the discrete space.

As a particular case, consider a wave propagation problem where a crack is present in the coupling interface between a bilayered material. If the main purpose of the numerical simulation is the identification the presence of a crack, then the PUFEM discretization should only include those eigenmodes which are able to detect and observe the crack. So, limiting the number of modes involved in the discretization will reduce the size of the matrix linear systems and keep bounded its condition number.

A detailed numerical study of crack phenomena is beyond the scope of this work since, even in the simplest planar and two-dimensional setting, a variety of crack parameters can be studied, such as the positions of the starting and ending points, its length, etc. However, following the methodology used in [5], it is possible to define a criterion to quantify the ability of an eigenmode to observe a crack using the following two indicators O_1 and O_2 :

$$O_1(n, j) = \left| \int_{\Omega} q_j(x_1) p_{n,j}(x_2) T_1(x_1, x_2) dx_1 dx_2 \right|, \quad (45)$$

$$O_2(n, j) = \left| \int_{\Omega} q_j(x_1) p_{n,j}(x_2) T_2(x_1, x_2) dx_1 dx_2 \right|, \quad (46)$$

with $n, j \in \mathbb{N}$, and where $q_j \otimes p_{n,j}$ is a Love or interior eigenmode (used in the modal-based PUFEM discretization), and $T_1 = S_A^* + S_B^*$ and $T_2 = S_A^* - S_B^*$. Functions S_A^* and S_B^* are the so-called singular dual functions associated with the crack, which are static extensions of the singular solutions of the scattered fields computed in the present of a crack. More precisely, if a crack with endpoints A

and B is placed on the coupling interface of the layered material, then

$$S_B^*(x_1, x_2) = \eta_B(r_B) S_{B_{\text{loc}}}^*(r_B, \theta_B) + S_{B_{\text{ext}}}^*(x_1, x_2)$$

where η_B is a cut-off function centered at the crack tip B with support contained in a disc D_B of radius R_B , (r_B, θ_B) are the local polar coordinates centered at point B ,

$$S_{B_{\text{loc}}}^*(r_B, \theta_B) = \frac{1}{c^2} \left(\frac{1}{\sqrt{r_B}} - \frac{\sqrt{r_B}}{R_B} \right) \sin \left(\frac{\theta_B}{2} \right),$$

and finally $S_{B_{\text{ext}}}^* \in H^1(\Omega)$ is the solution (defined up to a constant) of the following problem:

$$\begin{cases} -\text{div}(c^2 \nabla S_{B_{\text{ext}}}^*) = c^2 \nabla \eta_B \cdot \nabla S_{B_{\text{loc}}}^* + \text{div}(c^2 S_{B_{\text{loc}}}^* \nabla \eta_B) & \text{in } \Omega \setminus D_B, \\ \frac{\partial S_{B_{\text{ext}}}^*}{\partial \mathbf{v}} = 0 & \text{on } \partial \Omega \setminus \partial D_B, \\ S_{B_{\text{ext}}}^* = 0 & \text{on } \partial D_B. \end{cases} \quad (47)$$

An analogous definition is also valid for S_A^* (see [5, Section 4.3] for a more detailed discussion).

An standard piecewise linear finite element discretization on a triangular mesh has been used to compute the solutions of $S_{A_{\text{ext}}}^*$ and $S_{B_{\text{ext}}}^*$, since no time-harmonic wave propagation phenomena is involved in their definitions (in fact, problem (47) is elliptic). Plots on Figure 13 show the singular dual functions S_A^* and S_B^* for a crack placed on the coupling interface lying on $x_2 = 0$ between two layers with tips at points $A = (0.6, 0)$ and $B = (0.8, 0)$.

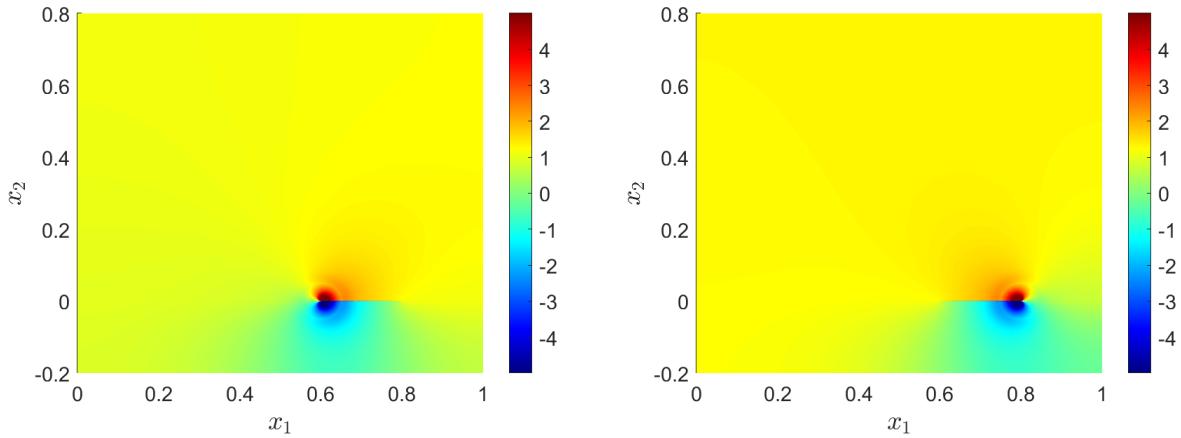


Figure 13: Singular dual functions S_A^* (left) and S_B^* (right) associated respectively with the endpoints A and B of the crack. The crack is set on the coupling interface between $x_2 = 0.6$ and 0.8 .

The computation of indicators $O_1(n, j)$ and $O_2(n, j)$ have been performed interpolating the closed-form expressions of the Love and interior eigenmodes using local high-order polynomial spaces in every mesh element (in particular, using \mathbb{P}^6 -polynomials). Plots in Figure 14 show the values of both indicators. The dashed line separate the Love eigenmodes (with smaller index j) from the interior modes (with larger values of index j). For observability purposes, these plots illustrate that it is enough to consider the Love and interior eigenmodes with n smaller than 15.

Notice also that for $n < 15$, the indicator values follow a decreasing trend as soon as n and j are increased, but their j -index decay is slower than in the n -index direction.

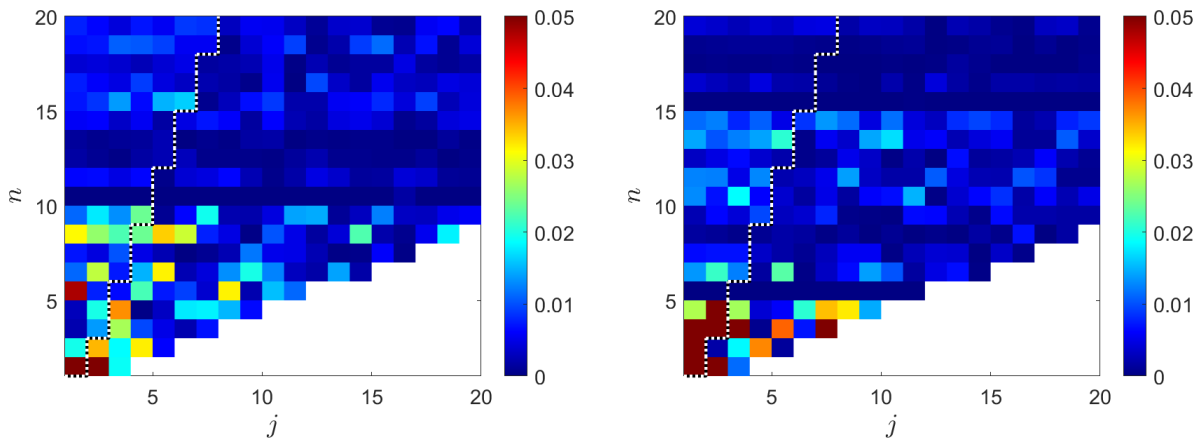


Figure 14: The two observability indicators O_1 (left) and O_2 (right) for a bilayered material plotted with respect to the indices n and j . The crack is set on the coupling interface between $x_2 = 0.6$ and 0.8 . The dashed line separates the Love modes (smaller j -index) from the interior modes (larger j -index).

7. Conclusions

In this manuscript, a non destructive testing problem in a bilayered domain without a crack has been studied. A modal-based partition of unity finite element method, using Love and interior modes to approximate the solution of the problem, has been proposed and described in detail. The high condition number associated with the discrete matrix have been also analysed. Finally, some numerical results have been presented in order to illustrate the accuracy of the method, the the numerical behaviour of the modal-based PUFEM results with respect to its condition number (using both LU-solvers and different regularization techniques). Additionally, it has been studied a feasible criterion to select a reduced basis in the modal-based PUFEM discrete space based on the observability of a crack placed on the coupling boundary between layers.

Acknowledgments

This work has been supported by Xunta de Galicia project “Numerical simulation of high-frequency hydro-acoustic problems in coastal environments - SIMNUMAR” (EM2013/052), co-funded with European Regional Development Funds (ERDF). Moreover, the second and fifth authors have been supported by MICINN projects MTM2014-52876-R, MTM2017-82724-R, PID2019-108584RB-I00, and also by ED431C 2018/33 - M2NICA (Xunta de Galicia & ERDF) and ED431G 2019/01 - CITIC (Xunta de Galicia & ERDF). Additionally, the third author has been supported by Junta de Castilla y León under projects VA024P17 and VA105G18, co-financed by ERDF funds.

References

- [1] R. Albanese, G. Rubinacci, and F. Villone. An integral computational model for crack simulation and detection via eddy currents. *Journal of Computational Physics*, 152(2):736–755, 1999.

- [2] G. Capuano, M. Ruzzene, and J. J. Rimoli. Modal-based finite elements for efficient wave propagation analysis. In *ASME 2013 International Design Engineering Technical Conferences and Computers and Information in Engineering Conference*. American Society of Mechanical Engineers, 2013.
- [3] K. Christodoulou, O. Laghrouche, M. S. Mohamed, and J. Trevelyan. High-order finite elements for the solution of Helmholtz problems. *Computers & Structures*, 191:129–139, 2017.
- [4] J. Davies and P. Cawley. The application of synthetic focusing for imaging crack-like defects in pipelines using guided waves. *IEEE Transactions on Ultrasonics, Ferroelectrics, and Frequency Control*, 56(4):759–771, 2009.
- [5] P. Destuynder and C. Fabre. Can we hear the echos of cracks? *Journal of Elasticity*, 130(1):25–58, 2018.
- [6] G. Diwan. *Partition of Unity Boundary Element and Finite Element Method: Overcoming Nonuniqueness and Coupling for Acoustic Scattering in Heterogeneous Media*. PhD thesis, Durham University, 2014.
- [7] G.C. Diwan, M.S. Mohamed, M. Seaid, J. Trevelyan, and O. Laghrouche. Mixed enrichment for the finite element method in heterogeneous media. *International Journal for Numerical Methods in Engineering*, 101(1):54–78, 2015.
- [8] T. Dogaru, C.H. Smith, R.W. Schneider, and S.T. Smith. Deep crack detection around fastener holes in airplane multi-layered structures using GMR-based eddy current probes. In *AIP Conference Proceedings*, volume 700, pages 398–405. American Institute of Physics, 2004.
- [9] J. C. Dumont-Fillon. *Contrôle Non Destructif par les Ondes de Love et Lamb*. Editions techniques de l'ingénieur, 2012.
- [10] A. Ern and J.-L. Guermond. *Theory and Practice of Finite Elements*. Applied Mathematical Sciences 159. Springer-Verlag New York, 1 edition, 2004.
- [11] S. Gopalakrishnan, A. Chakraborty, and D. R. Mahapatra. *Spectral Finite Element Method: Wave Propagation, Diagnostics and Control in Anisotropic and Inhomogeneous Structures*. Springer Science & Business Media, 2007.
- [12] S. Gupta, R. Dutta, and S. Das. Love-type wave propagation in an inhomogeneous cracked porous medium loaded by heterogeneous viscous liquid layer. *Journal of Vibration Engineering & Technologies*, pages 1–16, 2020.
- [13] L. Hervella-Nieto, P. M. López-Pérez, and A. Prieto. Robustness and dispersion analysis of the Partition of Unity Finite Element Method applied to the Helmholtz equation. *Computers & Mathematics with Applications*, 79(8):2426–2446, 2020.
- [14] F. Ihlenburg and I. Babuška. Dispersion analysis and error estimation of Galerkin finite element methods for the Helmholtz equation. *International Journal for Numerical Methods in Engineering*, 38(22):3745–3774, 1995.

- [15] F. Ihlenburg, I. Babuška, and S. Sauter. Reliability of finite element methods for the numerical computation of waves. *Advances in Engineering Software*, 28(7):417–424, 1997.
- [16] K.V. Kumar, T. J. Saravanan, R. Sreekala, N. Gopalakrishnan, and K.M. Mini. Structural damage detection through longitudinal wave propagation using spectral finite element method. *Geomechanics and Engineering*, 12(1):161–183, 2017.
- [17] O. Laghrouche and M.S. Mohamed. Locally enriched finite elements for the Helmholtz equation in two dimensions. *Computers & Structures*, 88(23-24):1469–1473, 2010.
- [18] A. J. Laub. *Matrix Analysis for Scientists and Engineers*. SIAM, 2005.
- [19] P.M. López-Pérez. *Numerical Study of Time-Harmonic Acoustic Problems in Layered Media Using Partition of Unity Finite Element Methods*. PhD thesis, Universidade da Coruña, 2017.
- [20] M. Malek, N. Izem, M. Seaid, M. S. Mohamed, and M. Wakrim. A partition of unity finite element method for nonlinear transient diffusion problems in heterogeneous materials. *Computational and Applied Mathematics*, 38(2):31, 2019.
- [21] J. M. Melenk. *On Generalized Finite Element Methods*. PhD thesis, University of Maryland, 1995.
- [22] J. M. Melenk and I. Babuška. The partition of unity finite element method: basic theory and applications. *Computer Methods in Applied Mechanics and Engineering*, 139(1):289–314, 1996.
- [23] M. S. Mohamed, O. Laghrouche, and A. El-Kacimi. Some numerical aspects of the pufem for efficient solution of 2d helmholtz problems. *Computers & Structures*, 88(23-24):1484–1491, 2010.
- [24] E. Perrey-Debain, O. Laghrouche, P. Bettess, and J. Trevelyan. Plane-wave basis finite elements and boundary elements for three-dimensional wave scattering. *Philosophical Transactions of the Royal Society of London A: Mathematical, Physical and Engineering Sciences*, 362(1816):561–577, 2004.
- [25] D. Royer and E. Dieulesaint. *Elastic Waves in Solids I: Free and Guided Propagation*. Springer Science & Business Media, 1999.
- [26] G. Seriani and E. Priolo. Spectral element method for acoustic wave simulation in heterogeneous media. *Finite Elements in Analysis and Design*, 16(3-4):337–348, 1994.
- [27] L. N. Trefethen and M. Embree. *Spectra and Pseudospectra: the Behavior of Nonnormal Matrices and Operators*. Princeton University Press, 2005.
- [28] R.P. Yadav, A.K. Singh, and A. Chattopadhyay. Analytical study on the propagation of rectangular semi-infinite crack due to Love-type wave propagation in a structure with two dissimilar transversely isotropic layers. *Engineering Fracture Mechanics*, 199:201–219, 2018.

- [29] M. H. Zarifi, S. Deif, M. Abdolrazzaghi, B. Chen, D. Ramsawak, M. Amyotte, N. Vahabisani, Z. Hashisho, W. Chen, and M. Daneshmand. A microwave ring resonator sensor for early detection of breaches in pipeline coatings. *IEEE Transactions on Industrial Electronics*, 65(2):1626–1635, 2017.